G：膨潤土內氣體傳輸行為

G.1：Paper－Development of numerical simulation method for gas migration through highly-compacted bentonite using model of two-phase flow through deformable porous media (ICEM 2010-40012)

Proceedings of the ASME 13th International Conference on Environmental Remediation and Radioactive Waste Management
ICEM2010
October 3-7, 2010, Tsukuba, Japan

ICEM2010-40011

GAS MIGRATION MECHANISM OF SATURATED HIGHLY-COMPACTED BENTONITE AND ITS MODELING

Yukihisa Tanaka
Central Research Institute of Electric Power Industry
Abiko-shi, Chiba-ken, Japan

Michihiko Hironaga
Central Research Institute of Electric Power Industry
Abiko-shi, Chiba-ken, Japan

Koji Kudo
Central Research Institute of Electric Power Industry
Abiko-shi, Chiba-ken, Japan

ABSTRACT

In the current concept of repository for radioactive waste disposal, compacted bentonite will be used as an engineered barrier mainly for inhibiting migration of radioactive nuclides. Hydrogen gas can be generated inside the engineered barrier by anaerobic corrosion of metals used for containers, etc. If the gas generation rate exceeds the diffusion rate of gas molecules inside of the engineered barrier, gas will accumulate in the void space inside of the engineered barrier until its pressure becomes large enough for it to enter the bentonite as a discrete gaseous phase. It is expected to be not easy for gas to entering into the bentonite as a discrete gaseous phase because the pore of compacted bentonite is so minute. Therefore the gas migration tests are conducted in this study to investigate the mechanism of gas migration. On the basis of the experimental facts obtained through the gas migration tests, possible gas migration mechanism is proposed. A simplified method for calculating gas pressure at large breakthrough, which is defined as a sudden and sharp increase in gas flow rate out of the specimen is also proposed.

Bentonite, gas migration, laboratory experiment, modeling

INTRODUCTION

In the current concept of repository for radioactive waste disposal, compacted bentonite will be used as an engineered barrier mainly for inhibiting migration of radioactive nuclides [1][2][3]. Hydrogen gas can be generated inside the engineered barrier by anaerobic corrosion of metals used for containers, etc. If the gas generation rate exceeds the diffusion rate of dissolved gas inside of the engineered barrier, gas will accumulate in the void space inside of the engineered barrier until its pressure becomes large enough for it to enter the bentonite as a discrete gaseous phase. It is expected to be not easy for gas to entering into the bentonite as a discrete gaseous phase because the pore of compacted bentonite is so minute. Therefore it is necessary to evaluate the effect of the accumulated gas pressure on surrounding objects such as concrete lining, rock mass and to evaluate volume of gas and water drained from the compacted bentonite by the accumulated gas pressure. It is also necessary to evaluate the effect of gas breakthrough on the barrier function of the compacted bentonite. To solve these problems, it is basically necessary to reveal and to model gas migration mechanism. Experimental studies as well as modeling have been conducted to investigate and to model gas migration phenomenon in compacted bentonite [4][5][6][7][8]. Numerical simulation analyses using various kinds of gas migration models were conducted for the results of the large scale model test for gas migration [9].

Table1 Test cases of the gas migration test

Case No.	Dry Density (Mg/m^3)	Specimen Size		Measured values	
		Diameter (mm)	Height (mm)	Swelling pressure (MPa)	Hydraulic coductivity (m/s)
No.1	1.218	60	20	0.390	7.08×10^{-13}
No.2	1.202	60	20	0.391	7.25×10^{-13}
No.3	1.407	60	20	0.698	3.70×10^{-13}
No.4	1.392	60	20	0.637	3.79×10^{-13}
No.5	1.585	60	20	1.733	1.43×10^{-13}
No.6	1.607	60	20	1.854	1.40×10^{-13}
No.7	1.423	200	20	0.720	3.71×10^{-13}
No.8	1.391	200	20	0.639	4.29×10^{-13}

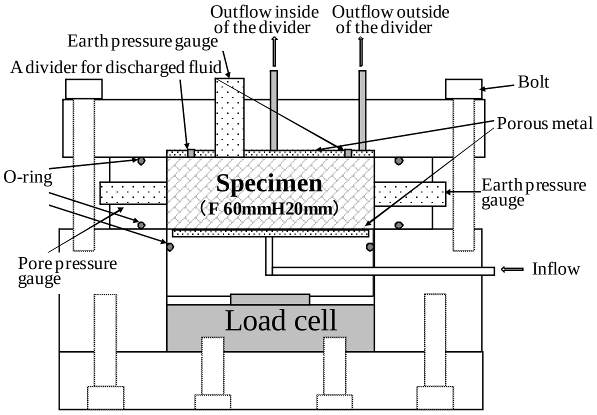

(a) A section in direction of the cylinder axis

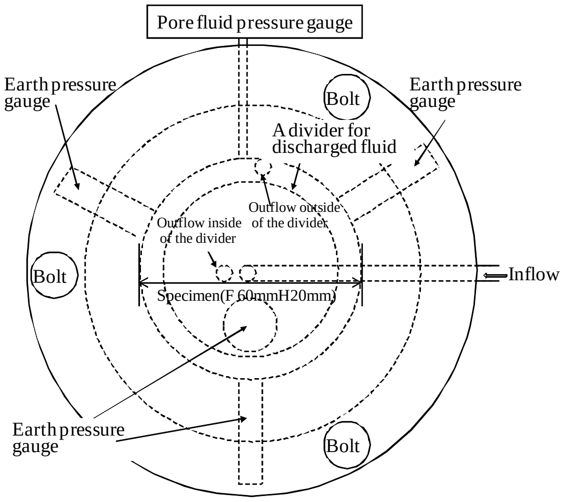

(b) A section perpendicular to the cylinder axis

Fig.1 Sections of specimen cells used for the gas migration test from Case No.1 to CaseNo.6

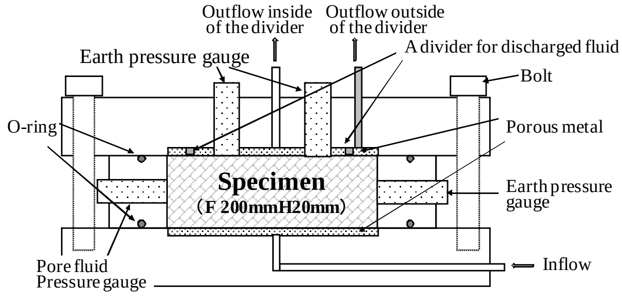

(a) A section in direction of the cylinder axis

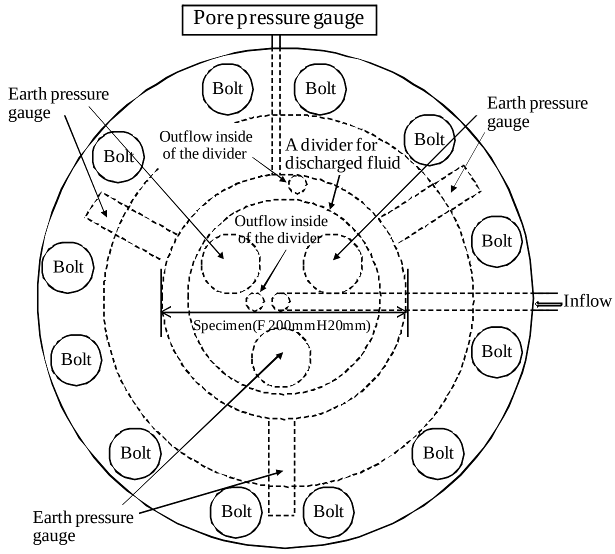

(b) A section perpendicular to the cylinder axis

Fig.2 Sections of specimen cells used for the gas migration test from Case No.7 to Case No.8

However, all the parameter which were used for these analyses, were not determined based on clear physical grounds.

In this paper, judging that relevance of gas migration analysis for the gas migration model test is ambiguous because gas migration mechanism is not clear yet even in small-sized specimen tests, precise experiments of gas migration tests using small-sized specimens are conducted for clarify gas migration mechanism of saturated highly compacted bentonite. A method for evaluating gas pressure at large breakthrough, which is defined as a sudden and sharp increase in gas flow rate out of the specimen, is proposed.

GAS MIGRATION TEST

Measurement of volume of discharged pore water and gas during the gas migration test is necessary for assessment of leakage of nuclides. Measurement of earth pressure is necessary for evaluating earth pressure acting on facilities for radioactive waste disposal. Furthermore, hydraulic conductivity of the specimen after large breakthrough is also important because of assessing low permeability of engineered barrier after large breakthrough. Therefore, hydraulic conductivity of the specimen is also measured before and after large breakthrough.

Test conditions

Table 1 shows test cases of the gas migration test conducted in this study. In the test cases from No.1 to No.6, the effect of dry density of the specimen on the gas migration characteristics is investigated, while the effect of diameter of the specimen on the gas migration characteristics are investigated comparing the

Table 2 Properties Bentonites used in this study

Type	Sodium bentonite
Specific gravity of soil particle	2.78 (Mg/m^3)
Montmorillonite content [Note1)]	50 (%)
Cation exchange capacity[Note2)]	1.040 (mequiv./g)
Capacity of exchangeable Na ion[Note3)]	0.611 (mequiv./g)
Capacity of exchangeable Ca ion[Note3)]	0.389 (mequiv./g)
Capacity of exchangeable K ion[Note3)]	0.024 (mequiv./g)
Capacity of exchangeable Mg ion[Note3)]	0.015 (mequiv./g)

Note1) Estimated by amount of absorption of methylene blue

Note2) The sum total of excahangeable Na ion, Ca ion, K ion and Mg ion capacity

Note3) Estimated by extraction using 1N-CH_3COONH_4

results of test cases No.7 and No.8 with those of test cases No.3 and No.4.

Figs 1 and 2 shows cross sections of an experimental cell which is made basically of stainless steel. Volume of discharged water and gas can be measured by porous metal which is divided into two pieces by a divider to allow volume of discharged water and gas near the inner wall of the vessel are measured. The divider is called ring in this paper. The dividers of 1mm in thickness are placed at 24.5 mm, 90.5 mm from the centre of the specimen of the test cases from No.1 to No.6 and the test cases from No.7 to No.8, respectively. Axial stress is measured by both a load cell and an earth pressure gauge, while radial stress and pore fluid pressure are measured by three earth pressure gauges and a pore pressure gauge, respectively. Table 2 shows basic properties of bentonite used in this study. Powdered bentonite is statically compacted at natural water content ranging from 7.2% to 9.9% to form specimens.

Pressurization

Water pressure is applied to the lower end of the compacted bentonite specimen for about 110 days to let water infiltrate through the specimen for complete water saturation. Swelling pressure and hydraulic conductivity in Table 1 are measured after infiltration of water. At the end of infiltration, hydraulic conductivity written in Table 1 is measured. After exchanging the lower wet porous metal for a dry porous metal, air pressure of 0.3 MPa, water pressure of 0.3 MPa are applied as back pressure to lower end of the specimen, upper end of the specimen, respectively. This state of stresses is called initial state in this paper. Gas migration tests start from this state. Swelling pressure at initial state is written in Table 1.

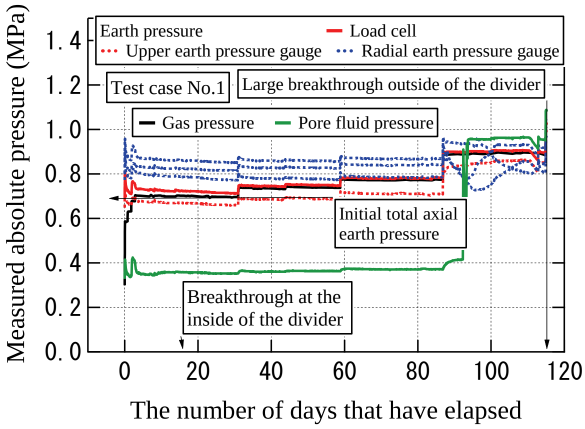

(a) Gas pressure, earth pressure and pore fluid pressure

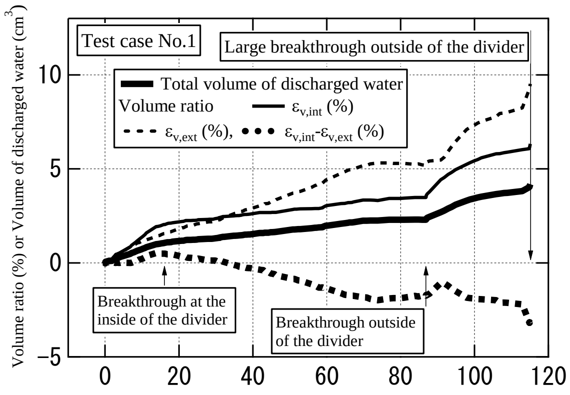

(b) Volume of discharged water

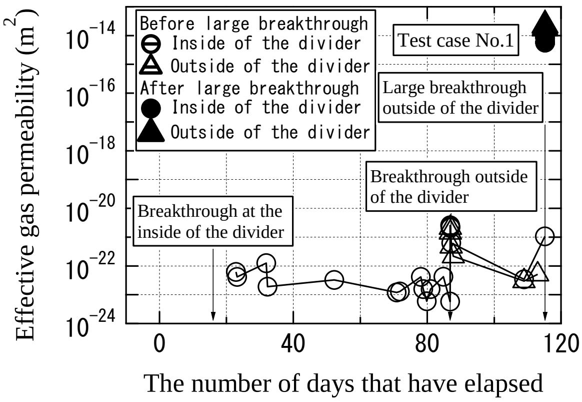

(c) Effective gas permeability

Fig.3 Change of measured values with the passage of time (Test case No.1)

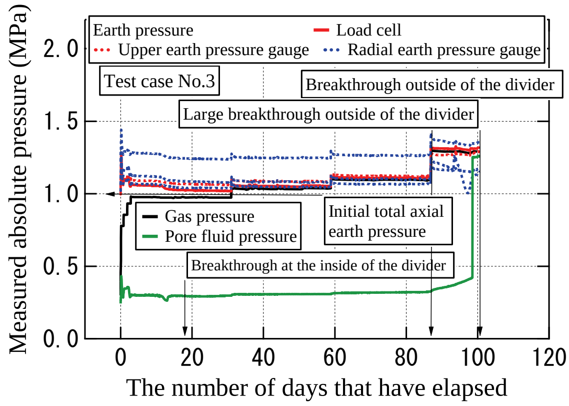

(a) Gas pressure, earth pressure and pore fluid pressure

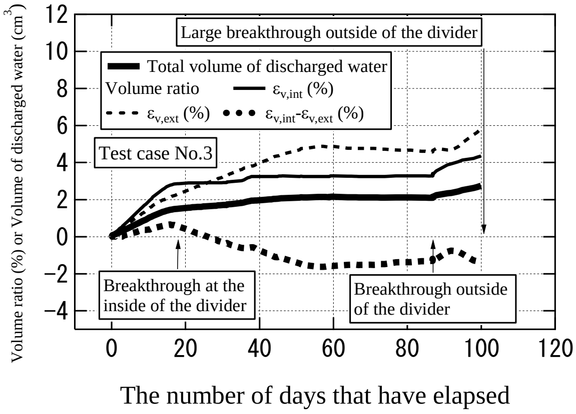

(b) Volume of discharged water

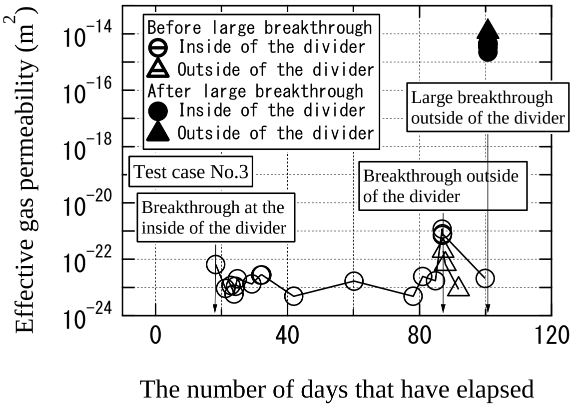

(c) Effective gas permeability

Fig.4 Change of measured values with the passage of time (Test case No.3)

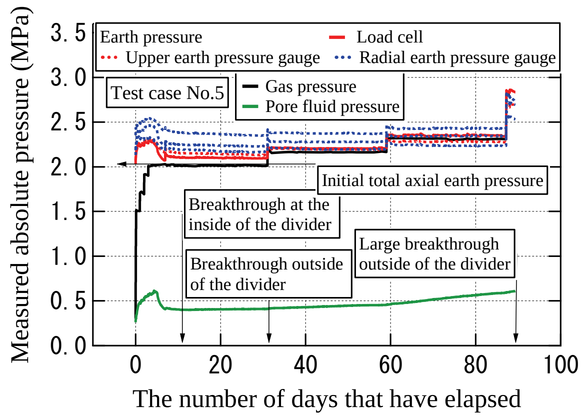

(a) Gas pressure, earth pressure and pore fluid pressure

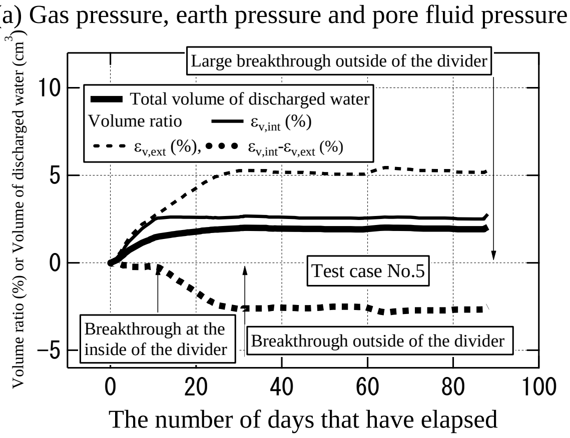

(b) Volume of discharged water

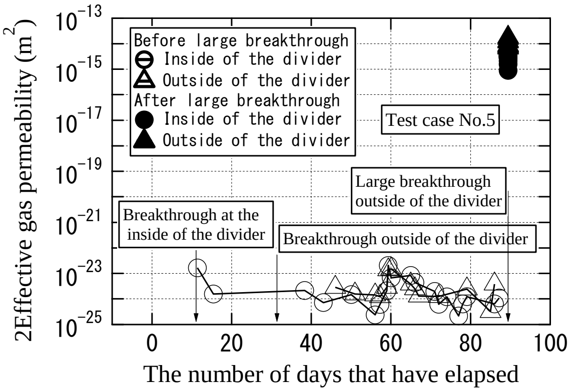

(c) Effective gas permeability

Fig.5 Change of measured values with the passage of time (Test case No.5)

THE TEST RESULTS AND CONSIDERATION

Behavior of specimen during pressurization and proposal of gas migration mechanism

Figs.3, 4, 5 and 6 show examples of results of the gas migration test, showing change of gas pressure, earth pressure, pore fluid pressure, volume of discharged water and effective gas permeability with the passage of time. Breakthrough of gas,

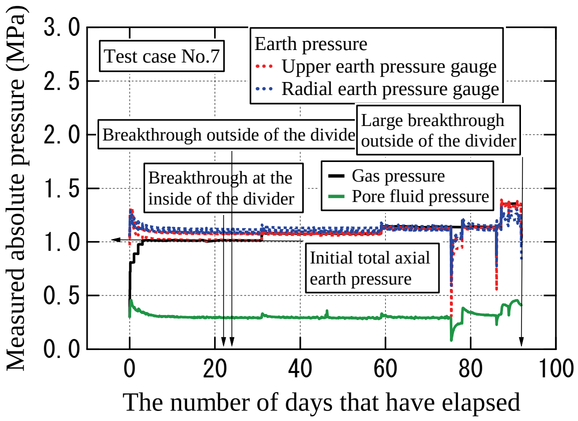

(a) Gas pressure, earth pressure and pore fluid pressure

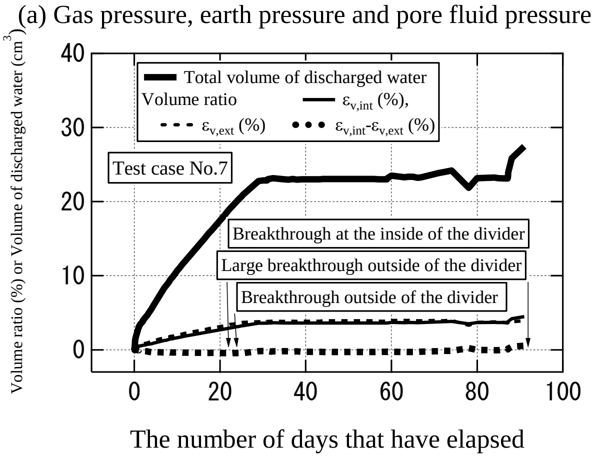

(b) Volume of discharged water

Fig.6 Change of measured values with the passage of time (Test case No.7)

which is defined as appearance of bubbles in the semitransparent drainage tube, occurs when applied gas pressure is equal to the initial total axial stress or somewhat smaller. By increasing the gas pressure more, large breakthrough of gas, which is defined as a sudden and sharp increase in gas flow rate out of the specimen, occurs. When the total gas pressure exceeds the initial total axial stress, the total axial stress is always equal to the total gas pressure because specimens shrink in the axial direction with causing the clearance between the end of the specimen and the lower porous metal as illustrated in Fig.7.

Effective gas conductivity, which is defined by Eq.(1), after the large breakthrough is ranging from 10^8 to 10^{10} times larger than that measured before the large breakthrough of gas migration.

$$K = \frac{Q\mu H P_1}{A} \cdot \frac{2}{\{P_{in}(t)\}^2 - \{P_{out}\}^2} \qquad (1)$$

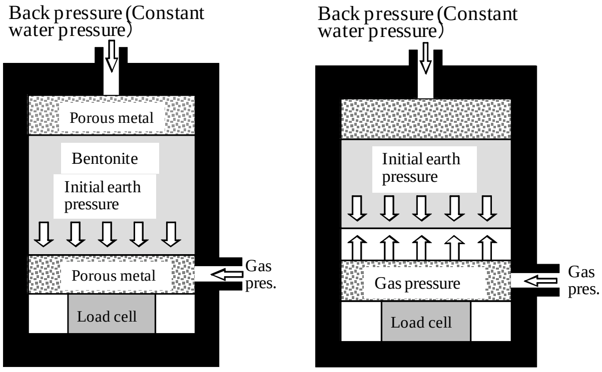

(a) Gas pres.<Initial total pres. (b) Gas pres.>Initial total pres.

Fig.7 Shrinkage of specimen due to gas pressure over initial axial total stress

where, K_g : effective gas permeability, Q : flow rate of gas in a normal state (Nm^3/s), μ : coefficient of viscosity, P_{in} : inflow gas pressure (Pa), P_{out} : outflow gas pressure (Pa), A : area of radial section of the specimen (m^2), H : height of the specimen (m), P_1 : atmospheric pressure

This fact means that the large breakthrough of gas migration is effective in reducing gas pressure accumulated in the vault for radioactive waste disposal and that the large breakthrough must be accompanied by the damage, such as fissures, to the specimen.

Figs. 3(b), 4(b), 5(b) and 6(b) show volume change of discharged water with the passage of time. The internal volume ratio, $\varepsilon_{v,int}$, which is defined as volume of discharged water inside the divider divided by soil volume inside the divider and the external volume ratio, $\varepsilon_{v,ext}$, which is defined as volume of discharged water outside of the divider divided by soil volume outside of the divider, are also plotted in the graphs. According to Figs. 3(b), 4(b), 5(b) and 6(b) and their digital values, the following facts and consideration, which are concerned with gas migration mechanism of saturated highly compacted bentonite, can be drawn :

1) As soon as the gas pressure, which is initially equal of back pressure of 0.3 MPa, increases, discharge of water can be seen. This means gas entry pressures into the bentonite specimens are zero or very small.
2) For the first several days of pressurization, the external volume ratio equals the internal volume ratio. This means gas enters uniformly during this period of days.
3) After the first several days of pressurization, the internal volume ratio is larger than the external volume ratio before gas breakthrough inside of the ring. The preferential pathways of gas are formed. Since formation of the preferential pathways is accompanied by deformation of surrounding soil, the preferential pathways out of the ring

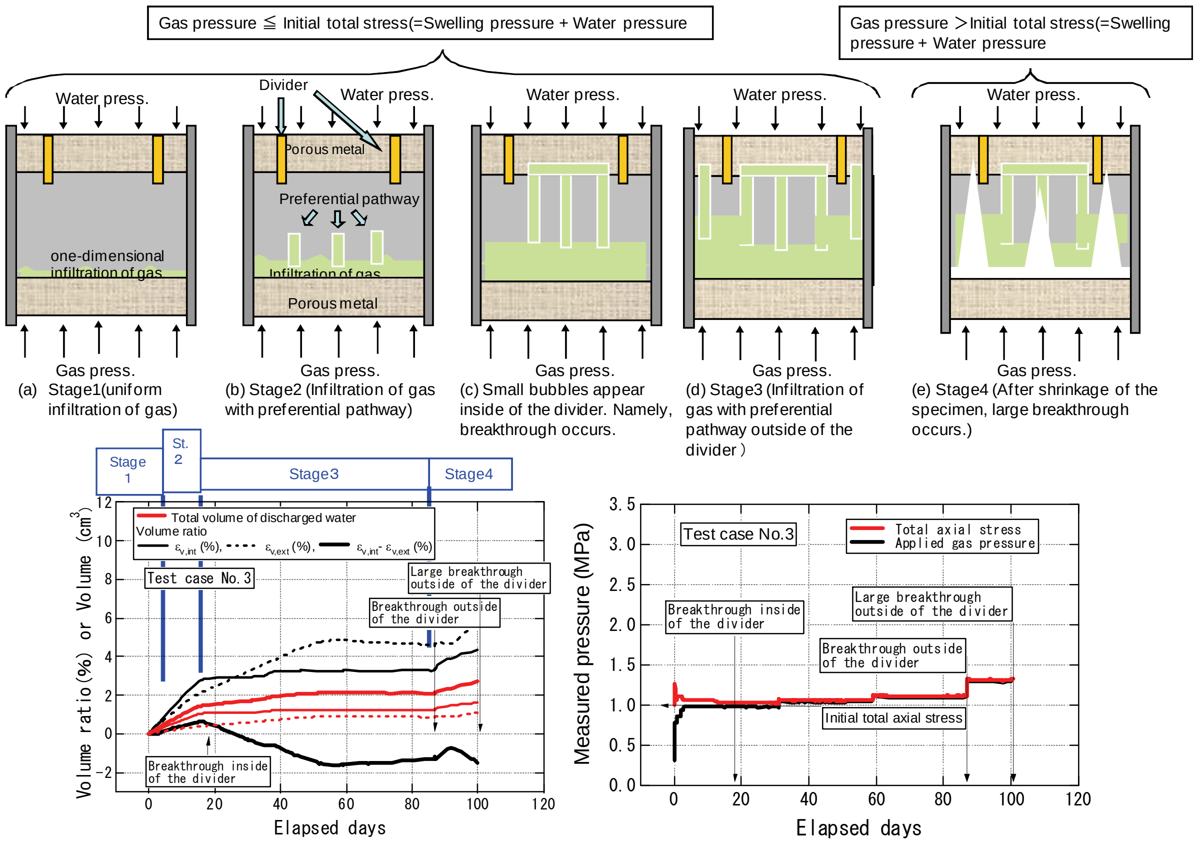

Fig.8 Estimated gas migration mechanism from the beginning of gas pressurization to large breakthrough

proceed more slowly because rigidity of the side wall of the cell prevent preferential pathways from forming.

4) After the breakthrough inside the ring, discharge of water inside the ring almost stops because the preferential pathway inside the ring reaches the upper end of the specimen.

Gas migration mechanism in highly-compacted bentonite mentioned above is shown in Fig.8 and summarized as follows :

1) At the very beginning of pressurization, gas enters the bentonite specimen uniformly.(See Fig.8(a)).
2) By increasing gas pressure after the very beginning of pressurization, preferential pathways are formed (See Fig.8(b)).
3) The preferential pathways inside of the ring proceed more rapidly than those out side of the ring.
4) After the preferential pathway inside the ring reaches the upper end of the specimen, discharge of water inside of the ring almost stops (See Fig.8(c)).
5) By increasing applied gas pressure to initial axial total earth pressure, the bentonite specimen begins to shrink in the axial direction with causing the clearance between the end of the specimen and porous metal (See Fig.8(e)).
6) By increasing applied gas pressure more beyond initial axial total earth pressure, large breakthrough occurs forming fissures in the bentonite specimen (See Fig. 8(e)).

Initial total earth pressure and its relation to breakthrough gas pressure and large breakthrough gas pressure

Figure 9 shows initial total earth pressure and its relation to gas pressure at breakthrough and large breakthrough. According to Figure 9, gas pressure, when the breakthrough inside the ring occurs, equals initial axial total earth pressure, while large breakthrough gas pressure is larger than the initial axial total earth pressure. It can be also said that the relationships shown in Fig.9 are not affected by the diameter of the specimen.

Relationship between dry density and effective gas permeability

Figure 10 shows the relation between dry density and effective gas permeability. Existing test results[4] are also plotted in Fig.10, indicating that effective gas permeability before large breakthrough, effective gas permeability after

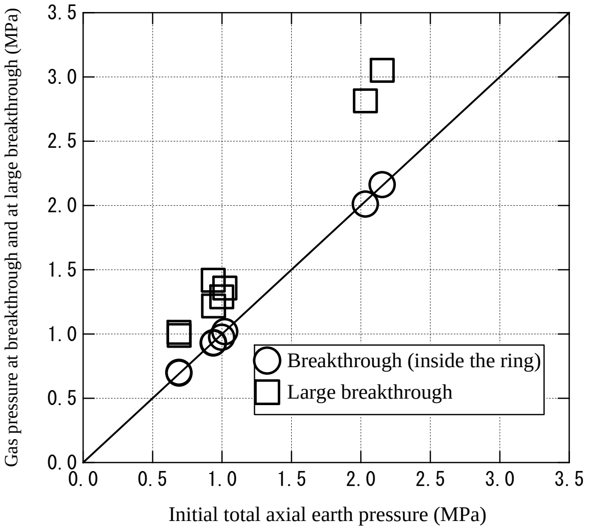

Fig.9 Gas pressure at breakthrough or at large breakthrough and their relation to initial total earth pressure

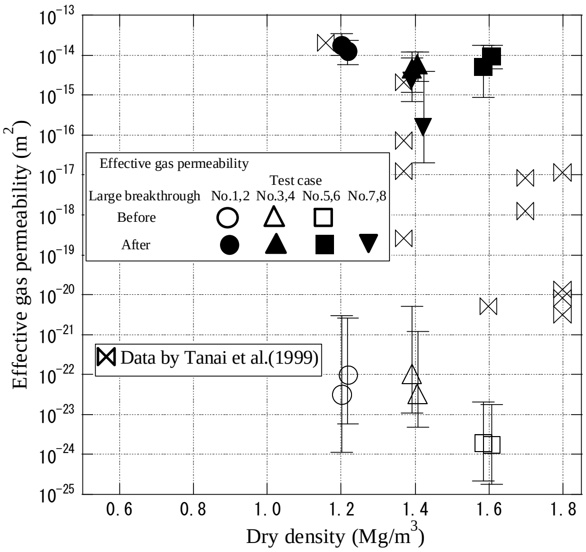

Fig.10 Relationship between effective gas permeability and dry density

large breakthrough are respectively approximate minimum, maximum of the data, irrespective of dry density as well as diameter of the specimen.

Comparison between hydraulic conductivity after large breakthrough and that before gas migration test

Figure 11 shows comparison between hydraulic conductivity after large breakthrough and that before gas migration test, indicating that hydraulic conductivity after large breakthrough is somewhat smaller than that before gas migration test. This means that the nature of very low hydraulic conductivity of highly compacted bentonite does not change substantially due to large breakthrough irrespective of dry density as well as diameter of the specimen.

A SIMPLIFIED METHOD FOR EVALUATING LARGE BREAKTHROUGH PRESSURE

As mentioned previously in this paper, large breakthrough is effective in reducing gas pressure accumulated in the vault of radioactive waste disposal. Thus, a simplified method for evaluating large breakthrough pressure is proposed herein.

Modeling large breakthrough

As described previously in this paper, large breakthrough must be caused by rupture of the specimen. Therefore, in this paper, hydraulic fracturing mechanism which is expressed by Eq.(2), is assumed. The hydraulic fracturing mechanism can be illustrated in Fig.12.

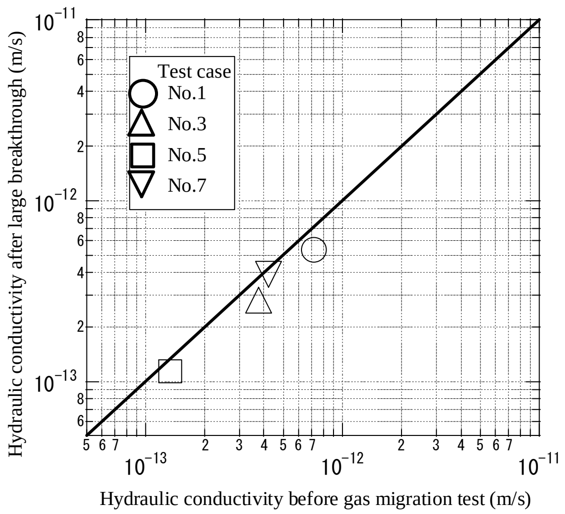

Fig.11 Change in hydraulic conductivity due to large breakthrough

$$P_g > \sigma'_r + u_w + \sigma'_t \quad (2)$$

where, P_{gas} : gas pressure, σ'_t : tensile strength, σ'_r : effective radial stress, u_w : pore water pressure

As illustrated in Fig.7, specimens shrink in axial direction with causing a gap between the end of the specimen and the lower porous metal. Shrinkage of specimens must be caused by theory of consolidation mechanism of soils. Therefore, stress state of specimens during shrinkage is estimated by one-dimensional consolidation theory. In this paper, for simplicity,

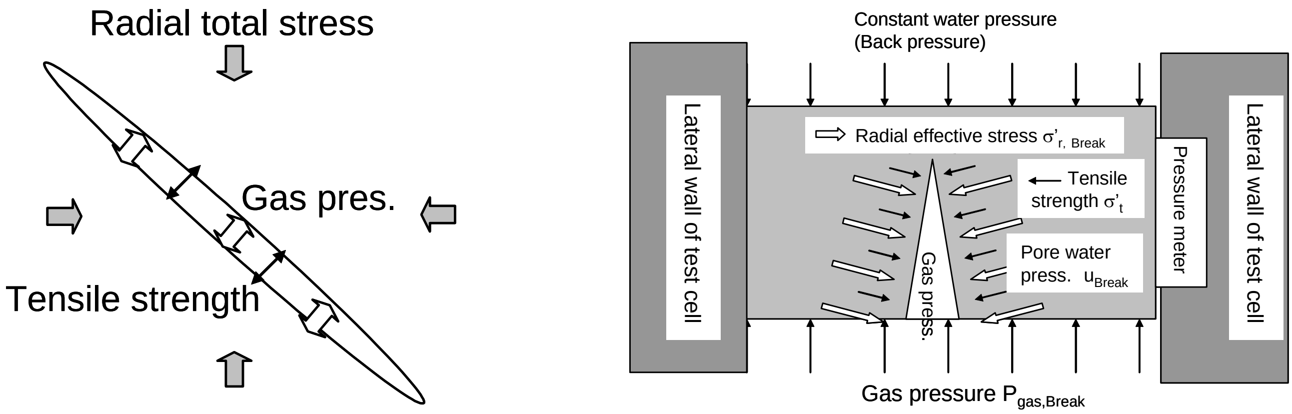

(a) A section perpendicular to the forward direction of the fissure (b) A section parallel to the forward direction of the fissure

Fig.12 Presumed state of stress around the fissure induced by the applied gas pressure

the specimens are assumed to be fully saturated throughout pressurization. Thus one-dimensional consolidation theory for fully saturated soils is used for calculation.

Further, assuming the fissure appears at the end of the specimen propagates in the specimen rapidly, the criteria of large breakthrough of the specimen is expressed by rewriting Eq.(2) as follows :

$$\Delta\sigma'_{a,end,Break} = \frac{\sigma'_t}{1-K_0} \tag{3}$$

where, $\Delta\sigma'_{a,end,Break}$: Increment of effective axial stress at the pressurized end of the specimen from initial effective axial stress, K_0 : coefficient of earth pressure at rest.

Coefficient of volume compressibility, m_v , in the one-dimensional consolidation theory, is calculated by the following equation :

$$m_v = -(\mathrm{d}\rho_{db}/\rho_{db})/\mathrm{d}P_s = -(\mathrm{d}\rho_{db}/\mathrm{d}P_s/\rho_{db}) \tag{4}$$

where, ρ_{db} : dry density of bentonite, P_s : swelling pressure

Comparison between calculated results and experimental results

Using one-dimensional consolidation theory, the values of $\Delta\sigma'_{a,end,Break}$ of the test cases in Table 1, which are calculated backwards from one-dimensional consolidation theory, are plotted in Fig.13 against their respective swelling pressures. Using Eq.(3), in which K_0=0.5 is assumed, and the average relationship in Fig.13, tensile strength in Eq. (2) is estimated.

Measured large breakthrough pressures of test in Table 1 are plotted against the calculated results in Fig.14, showing good agreement with calculated results.

Comparison between calculated results and experimental results is also conducted for test results by JAEA [4] shown in Table 3 which was conducted for specimens with various heights under various pressing speed. Figure 14 shows that the calculated results show good agreement with test results by JAEA. In this case, tensile strength in Eq. (2) is also estimated using Eq.(3), in which K_0=0.5 is assumed, and the average relationship in Fig.13. Good agreement between the calculated results and the experimental results can also be seen in Fig.15.

CONCLUSIONS

Firstly, the following conclusions were obtained through by the results of the gas migration tests which are conducted in this study:

1) Bubbles appear in the semitransparent drainage tube at first when the gas pressure is equal to the initial total axial stress or somewhat smaller. By increasing the gas pressure more, large breakthrough of gas migration, which defined as a sudden and sharp increase of amount of emission gas, occurred. When the total gas pressure exceeds the initial total axial stress, the total axial stress is always equal to the total gas pressure because specimens shrink in the axial direction with causing the clearance between the end of the specimen and porous metal.
2) Effective gas conductivity after large breakthrough of gas migration is ranging from 10^8 to 10^{10} times larger than that measured before the large breakthrough of gas migration. This fact means the large breakthrough is effective in

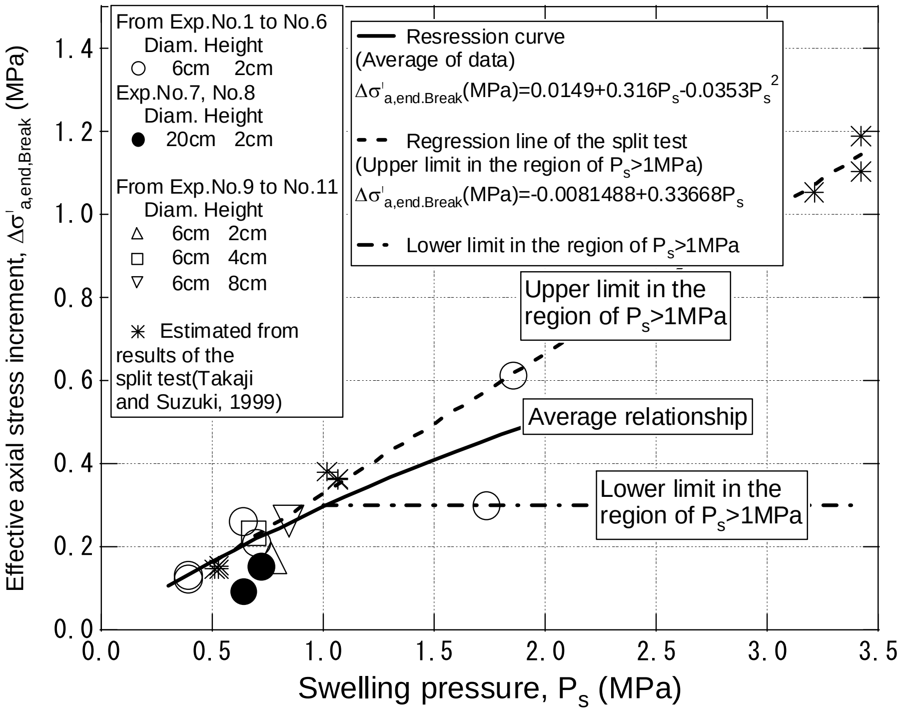

Fig.13 Relationship between swelling pressure and effective axial stress increment at the gas pressurized end of the specimen when gas breakthrough occurred

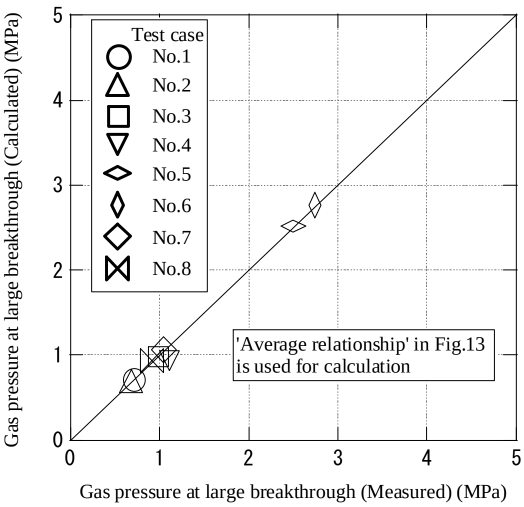

Fig.14 Relationship between measured results and calculated results of large gas breakthrough pressure (Test cases from No.1 to No.8)

reducing gas pressure accumulated in the vault for radioactive waste disposal.

3) On the basis of experimental facts, possible gas migration mechanism of dense bentonite is proposed.

Table 3 Test cases of gas migration test conducted by JAEA [4]

Test case No.	Dry density (Mg/m^3)	Pressing speed (MPa/day)	Specimen size	
			Diam. (mm)	Height (mm)
No.9	1.6	5.98×10^{-2}	50	10
No.10	1.6	1.92×10^{-1}	38	20
No.11	1.6	1.00×10^{-1}	50	30
No.12	1.6	6.86×10^{-2}	50	30
No.13	1.8	2.45×10^{-2}	50	10
No.14	1.8	1.22×10^{-2}	50	30
No.15	1.8	9.54×10^{-2}	50	30
No.16	1.8	1.42×10^{-1}	50	50
No.17	1.8	4.81×10^{-2}	50	50

Note : Gas pressure is applied to the applied to the specimen continuously.

4) Hydraulic conductivity of water measured after large breakthrough of gas migration is somewhat smaller than that measured before the gas migration test. This fact means that it might be possible to neglect decline of the function of bentonite as engineered barrier caused by large breakthrough of gas migration.

Secondly, the following conclusions were obtained by modeling breakthrough of gas migration:

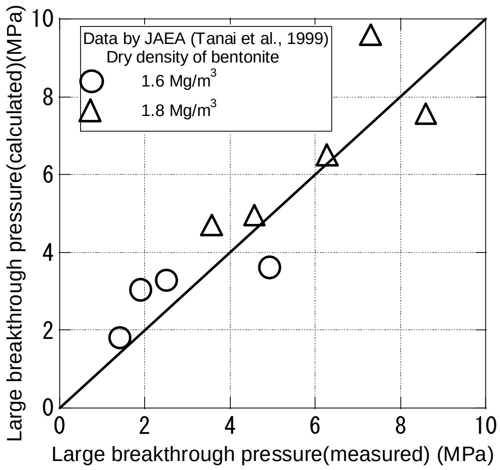

Fig.15 Comparison of the test results by JAEA with calculated results the methodology of which is proposed in this paper

5) The bentonite specimen shrinks in axial direction when total gas pressure exceeds initial total stress of the specimen. The phenomenon was modeled by one-dimensional consolidation theory so that it can be handled simply.
6) Stresses of bentonite specimen at large breakthrough of gas migration is estimated by reverse calculation of the test results. The estimated stresses are accordant with the stresses which estimated by assuming hydraulic fracturing mechanism. This fact means breakthrough of gas migration probably occurs according to the hydraulic fracturing mechanism.
7) The breakthrough pressure of gas migration is calculated by using the proposed relationship between swelling pressure and effective axial stress at breakthrough of gas migration. The calculated results show good agreement with not only test results obtained by this study but also those by other organization.

ACKNOWLEDGMENTS

This study was conducted by the request of The Federation of Electric Power Companies of Japan. The authors are grateful to the persons who gave assistance to this study, especially, Prof. M. Nishigaki (Okayama University) and Mr. K.Tanai (Japan Atomic Energy Agency) for their advice to gas migration characteristics of bentonite. The authors are also grateful to T. Yokokura (Ceres, Co., Ltd.) and I. Wakabayashi (C.P.C., Co., Ltd.) for assistance in conducting laboratory tests.

REFERENCES

[1] For example, JNC, 2005, H17 Development and management of the technical knowledge base for the geological disposal of HLW, Knowledge Management Report, JNC TN1400 2005-022. (in Japanese)
[2] For example, Subcommittee of subsurface radioactive disposal, Energy civil engineering committee , 2008, A way of determining parameters for evaluating migration of nuclides in the groundwater scenario, Japan Society of Civil Engineering. (in Japanese)
[3] For example, JAEA and FEPC, 2007, Second progress report on research and development for TRU waste disposal in Japan, － Repository design, safety assessment and means of implementation in the generic phase －, JAEA-Review 2007-010, FEPC TRU-TR2-2007-01. (in Japanese)
[4] Tanai, K., Sato, H., Murakami, T. and Inoue, M., 1999, A preliminary assessment of gas diffusion and migration (Research Report), JNC Tokai-jigyousyo, JNC TN8400 99-045. (in Japanese)
[5] Horseman, S.T., Harrington, J.F. and Sellin, P., 1999, Gas migration in clay barriers, Engineering Geology, **54**, pp.139-14.
[6] Graham, J., Halayko, K.G., Hume, H., Kirkham, T., Gray, M. and Oscarson, D., 2002, “A capillarity -advective model for gas break-through in clays,” Engineering Geology, **64**, pp.273-286.
[7] Harrington, J.F. and Horseman, S.T., 2003, Gas migration in KBS-3 buffer bentonite, Sensitivity of test parameters to experimental boundary conditions, SKB Technical Report, TR-03-02.
[8] Hoch, A.R., Cliffe, K.A., Swift, B.T. and Rodwell, W.R., 2004, Modelling gas migration in compacted bentonite : Gambit club Phase 3 Final Report, POSIVA 2004-02.
[9] For example, Mori, K., Tada, K., Tasaka, H., Okamoto, S. and Fujiwara, A., 2005, “A discussion of the applicability of water/air two-phase flow modeling to in-situ gas migration behavior in engineered barrier system,” Proc. of the 34 th Symposium on Rock Mechanics, pp.41 - 48. (in Japanese)
[10] Takaji, K. and Suzuki, H., 1999, Static mechanical properties of buffer material (Research Report), JNC Tokai-jigyousyo, JNC TN8400 99-041. (in Japanese)

G.2：Paper－Gas migration mechanism of saturated highly-compacted bentonite and its modeling (ICEM 2010-40011)

Proceedings of the ASME 13th International Conference on Environmental Remediation and Radioactive Waste Management
ICEM2010
October 3-7, 2010, Tsukuba, Japan

ICEM2010-40012

DEVELOPMENT OF NUMERICAL SIMULATION METHOD FOR GAS MIGTATION THROUGH HIGHLY-COMPACTED BENTONITE USING MODEL OF TWO-PHASE FLOW THROUGH DEFORMABLE POROUS MEDIA

Yukihisa Tanaka
Central Research Institute of Electric Power Industry
Abiko-shi, Chiba-ken, Japan

ABSTRACT

In the current concept of repository for radioactive waste disposal, compacted bentonite will be used as an engineered barrier mainly for inhibiting migration of radioactive nuclides. Hydrogen gas can be generated inside of the engineered barrier by anaerobic corrosion of metals used for containers, etc. It is expected to be not easy for gas to entering into the bentonite as a discrete gaseous phase because the pore of compacted bentonite is so minute. Therefore it is necessary to investigate the effect of gas pressure generation and gas migration on the engineered barrier, peripheral facilities and ground.

In this study, a method for simulating gas migration through the compacted bentonite is proposed. The proposed method can analyze coupled hydrological-mechanical processes using the model of two-phase flow through deformable porous media. Validity of the proposed analytical method is examined by comparing gas migration test results with the calculated results, which revealed that the proposed method can simulate gas migration behavior through compacted bentonite with accuracy.

Key Words : *bentonite, gas migration, two-phase flow, stress-strain relationship*

INTRODUCTION

In the current concept of repository for radioactive waste disposal, compacted bentonite will be used as an engineered barrier mainly for inhibiting migration of radioactive nuclides. Hydrogen gas can be generated inside of the engineered barrier by anaerobic corrosion of metals used for containers, etc. If the gas generation rate exceeds the diffusion rate of dissolved gas inside of the engineered barrier, gas will accumulate in the void space inside of the engineered barrier until its pressure becomes large enough for it to enter the bentonite as a discrete gaseous phase. It is expected to be not easy for gas to enter into the bentonite as a discrete gaseous phase because the pore of compacted bentonite is so minute. Therefore it is necessary to evaluate the effect of the accumulated gas pressure on surrounding objects such as concrete lining, rock mass and to evaluate volume of gas and water discharged from the compacted bentonite by the accumulated gas pressure. To solve these problems, the author already conducted gas migration tests of saturated highly compacted bentonite [1]. Moreover a numerical analysis method of gas migration is necessary for evaluating amount of discharged water and gas from the facility and for evaluating stresses around the facility considering the shape of the facility, initial conditions and boundary conditions. Numerical simulation analyses using various kinds of gas migration models were conducted for the results of the large scale model test for gas migration [2]. However, since the numerical analysis methods currently used for gas migration through compacted bentonite are mostly based on conventional two-phase flow model, equilibrium of forces is not considered. Thus, stresses, amount discharged water and gas induced by deformation of specimen can not be considered, resulting in erroneous estimation.

It seems effective to develop a finite element computer code for simulating gas migration in compacted bentonite based on the model of two-phase flow through deformable porous media for solving the problems mentioned above. Thus, in this study, the finite element computer code is developed. Furthermore, the validity of the code is investigated in this paper by comparing calculated results with results of gas migration tests.

EQUATIONS DESCRIBING GAS MIGRATION PHENOMENON

Continuity equation of water and that of gas considering deformation of bentonite specimen

In this paper, compressive stress, compressive strain as well as compressive pressure have plus signs.

Mass flow rate, Δq_{wm}, into the soil element, whose position coordinate is (x_1, x_2, x_3), is expressed as follows :

$$\Delta q_{wm} = -\rho_w \cdot m_w \cdot \Delta V \cdot \Delta t \tag{1}$$

where, ρ_w : density of water, Δt : time increment, ΔV : volume of soil element (=$\Delta x_1 \times \Delta x_2 \times \Delta x_3$), Δx_1 ,Δx_2, Δx_3 : length of the soil element in x_1-, x_2- and x_3-direction, respectively, m_w : outflow rate of water per unit volume of soil, which is expressed by the following equation using Darcy's law :

$$m_w = -\frac{1}{\rho_w} \cdot \frac{\partial}{\partial x_i}\left\{\rho_w \cdot k_w \cdot \frac{\partial}{\partial x_i}\left(\frac{u_w}{\rho_w \cdot g}\right)\right\} \tag{2}$$

where, k_w : hydraulic conductivity, u_w : pore water pressure, g : gravitational acceleration, Einstain's summation convention is used the right side of Eq.(2).

Assuming incompressibility of soil particles, the following equation holds :

$$\Delta V - \Delta V_s = n \cdot \Delta V \tag{3a}$$

$$\partial(\Delta V_s)/\partial t = 0 \tag{3b}$$

where, ΔV_s : volume of soil particles in the soil element, , n : porosity

Therefore, considering Eq.(3b), $\partial(\Delta V)/\partial t$ is expressed as follows :

$$\frac{\partial}{\partial t}(\Delta V) = \Delta V_s \cdot \frac{\partial}{\partial t}(1+e) = \frac{\Delta V}{1+e} \cdot \frac{\partial e}{\partial t} \cong -\Delta V \cdot \frac{\partial \varepsilon_v}{\partial t} \tag{4}$$

where, e : void ratio, ε_v : volumetric strain of soil

According to Eqs.(3a), (3b) and (4), mass increment of soil element, which has volume of ΔV, during time of Δt is expressed as follows :

$$\Delta t \cdot \frac{\partial}{\partial t}(n \cdot S_w \cdot \rho_w \cdot \Delta V) = \Delta t \cdot \Delta V \cdot \left\{n \cdot \rho_w \cdot \frac{\partial S_w}{\partial t} + n \cdot S_w \cdot \frac{\partial \rho_w}{\partial t} - (S_w \cdot \rho_w) \cdot \frac{\partial \varepsilon_v}{\partial t}\right\} \tag{5}$$

where, S_w : water saturation

According to the law of conservation of mass, the right side of Eq.(1) equals the right side of Eq.(5). Thus, the following equation is obtained :

$$m_w = -n \cdot \frac{\partial S_w}{\partial t} - n \cdot S_w \cdot \frac{1}{\rho_w}\frac{\partial \rho_w}{\partial t} + S_w \cdot \frac{\partial \varepsilon_v}{\partial t} \tag{6}$$

Using bulk modulus of water, K_w and pore water pressure, u_w, change of density of water is expressed as follows :

$$\mathrm{d}\rho_w / \rho_w = 1/K_w \cdot \mathrm{d}u_w \tag{7}$$

Substituting Eq.(7) into Eq.(6), continuity equation of water is obtained as follows :

$$m_w = -n \cdot \frac{\partial S_w}{\partial t} - n \cdot S_w \cdot \frac{1}{K_w} \cdot \frac{\partial u_w}{\partial t} + S_w \cdot \frac{\partial \varepsilon_v}{\partial t} \tag{8}$$

Substituting m_g, S_g, K_g and u_g into m_w, S_w, K_w and u_w in Eq.(8) respectively, the following equation is obtained as continuity equation of gas.

$$m_g = -n \cdot S_g \cdot \frac{1}{K_g} \cdot \frac{\partial u_g}{\partial t} - n \cdot \frac{\partial S_g}{\partial t} + S_g \cdot \frac{\partial \varepsilon_v}{\partial t} \tag{9}$$

where, u_g : gas pressure, K_g : bulk modulus of gas, S_g : gas saturation, m_g : outflow rate of gas per unit volume of soil , which is expressed by the following equation using Darcy's law :

$$m_g = -\frac{1}{\rho_g} \cdot \frac{\partial}{\partial x_i}\left\{\rho_g \cdot k_g \cdot \frac{\partial}{\partial x_i}\left(\frac{u_g}{\rho_w g}\right)\right\} \tag{10}$$

where, ρ_g : density of gas, u_g : pore gas pressure, k_g : coefficient of gas permeability

The relationship between water saturation, S_w, and gas saturation, S_g, is expressed as follows :

$$S_g = 1 - S_w \tag{11}$$

Further, differentiating Eq.(11) partially with respect to t, the following equation is obtained :

$$\partial S_g / \partial t = -\partial S_w / \partial t \tag{12}$$

Considering the Boyle's law, K_g is expressed as follows :

$$K_g = \frac{\Delta u_g}{\Delta V_g / V_{g0}} = \frac{(u_g + P_a) - (u_{g0} + P_a)}{(V_{g0} - V_g)/V_{g0}} = u_g + P_a \tag{13}$$

where, P_a : atmospheric pressure, V_g : volume of gas at gas pressure of u_g, u_{g0} : initial gas pressure, V_{g0} : volume of gas at gas pressure of u_{g0}, Δu_g : gas pressure increment, ΔV_g : gas volume increment

Substituting Eqs. (11), (12) and (13) into Eq.(9), the following equation is obtained :

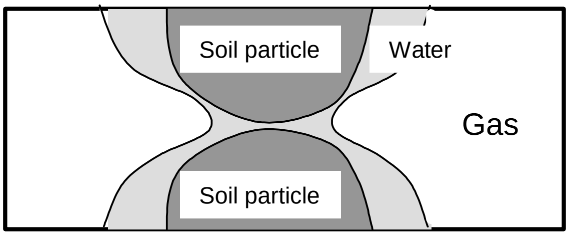

Fig.1 Assumed state of pore water near soil particles of bentonite

$$m_g = -\frac{n \cdot (1-S_w)}{u_g + P_a} \cdot \frac{\partial u_g}{\partial t} + n \cdot \frac{\partial S_w}{\partial t} + (1-S_w) \cdot \frac{\partial \varepsilon_v}{\partial t} \tag{14}$$

Relationships among dry density increment, porosity increment and volumetric strain increment

Since dry density change of the specimen is caused by volume change of the specimen during the gas migration test, there is the following relationship between dry density increment $d\rho_d$ and volumetric strain increment $\mathrm{d}\varepsilon_v$:

$$\mathrm{d}\rho_d = \rho_d \cdot \mathrm{d}\varepsilon_v \tag{15}$$

There is the following relationship between porosity increment dn and volumetric strain increment $\mathrm{d}\varepsilon_v$:

$$\mathrm{d}n = (n-1) \cdot \mathrm{d}\ \varepsilon_V \tag{16}$$

Equilibrium of forces

Equilibrium of forces is expressed as follows :

$$\partial \sigma_{ij} / \partial x_j + \rho \cdot b_i = 0 \tag{17}$$

where, ρ : wet density of bentonite, b_i : body force per unit mass in i-direction

Stress σ_{ij} in Eq. (17) is explained on the following.

a) Relationships among volumetric strain increment, mean effective stress increment and suction increment

A state of pore water around soil particles is assumed in Fig.1. According to Fig.1, strain of unsaturated soil is caused not only by externally applied stress but also by suction due to surface tension of water. Thus, strain of unsaturated soil is assumed to be divided into the following two classes :

1) Strain accompanied by inter-particle slippage caused by change in effective stresses
2) Strain , which is not accompanied by inter-particle slippage, caused by change in effective stresses

Thus, in this paper, Stress-strain relationship of unsaturated bentonite is assumed as follows :

$$\mathrm{d}\varepsilon_v = \mathrm{d}\sigma'_m / K_d(u_c) + S_w \cdot \mathrm{d}u_c / K_{dr} \tag{18a}$$

$$K_{dr} = K_{dr0} \cdot \left(\frac{\mathrm{Max}[\sigma'_m, u_c]}{P_a} \right) \tag{18b}$$

where, K_d : bulk modulus of the soil specimen in terms of effective stress, K_{dr} : bulk modulus of the soil specimen in terms of suction, K_{dr0} : a constant, σ_m, σ'_m : mean effective stress, mean total stress, respectively, u_c : suction (=u_g - u_w)

Assuming that suction u_c is given as a function of water saturation S_w , suction u_c is expressed as follows :

$$u_c = u_g - u_w = f(S_w) \tag{19}$$

The first term of the right-hand side of Eq.(18a) corresponds to strain 1) mentioned above while the second term of the right-hand side of Eq.(18a) corresponds to strain 2) mentioned above.

b) Three-dimensional stress-strain relationship

Since plastic strain seems to be not created in the specimen throughout the gas migration test because of small shear stress, the specimen is assumed to be an isotropic elastic body. Thus, $K_d(u_c)$ in Eq.(18a) is expressed as follows :

$$K_d(u_c) = E_d(u_c) / \{3 \cdot (1-\nu_d)\} \tag{20}$$

where, E_d, ν_d : Young's modulus, Poison's ratio of the soil specimen in terms of effective stress, respectively. Poison's ratio is assumed to be 0.3.

Eq.(18a) is rewritten as follows :

$$\mathrm{d}\sigma'_m = K_d(u_c) \cdot \mathrm{d}\varepsilon_v - K_d(u_c) \cdot S_w \cdot \mathrm{d}u_c / K_{dr} \tag{21}$$

Eq.(21) is further rewritten as a three-dimensional stress-strain relationship as follows :

$$\mathrm{d}\sigma_{ij} = \frac{E_d}{(1+\nu_d)} \cdot \mathrm{d}\varepsilon_{ij} + \delta_{ij} \cdot \frac{\nu_d \cdot E_d}{(1+\nu_d) \cdot (1-2\nu_d)} \cdot \mathrm{d}\varepsilon_{ll} + \delta_{ij} \cdot \mathrm{d}u - \delta_{ij} \cdot K_d(u_c) \cdot S_w / K_{dr} \cdot \mathrm{d}u_c \tag{22}$$

where, u : pore fluid pressure.

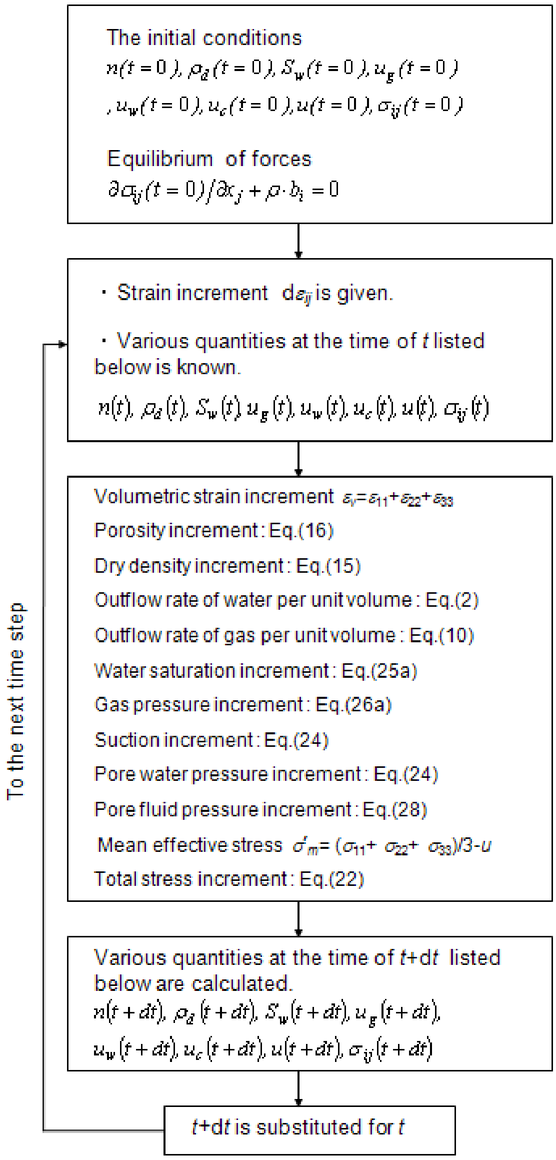

Fig.2 Procedure of gas migration analysis by the proposed method

Pore fluid pressure is defined as pressure obtained by taking stress transferred by a soil skeleton from total stress in this paper.

Pressure which is measured by pore pressure gauge shown in Fig.3 is regarded as pore fluid pressure. Further, since stress transferred by a soil skeleton is nothing but effective stress, the following equation holds :

$$\sigma_m = \sigma'_m + u \tag{23}$$

c) Increments of suction, water saturation, gas pressure and pore fluid pressure expressed by volumetric strain increment

Differentiating Eq.(19), the following equation is derived.

$$\mathrm{d}u_c = \mathrm{d}u_g - \mathrm{d}u_w = f'(S_w)\cdot \mathrm{d}S_w \tag{24}$$

By eliminating both du_g and du_w from Eqs.(8), (9) and (24) and by considering Eqs.(11) and Eq.(13), the following equation is obtained :

$$\mathrm{d}S_w = A_1(n,S_w,u_g)\cdot m_g + B_1(n,S_w,u_g)\cdot m_w + C_1(n,S_w,u_g)\cdot \mathrm{d}\varepsilon_v \tag{25a}$$

where,

$$A_1(n,S_w,u_g) = -(u_g + P_a)/(1-S_w)/F(n,S_w,u_g) \tag{25b}$$

$$B_1(n,S_w,u_g) = (K_w/S_w)/F(n,S_w,u_g) \tag{25c}$$

$$C_1(n,S_w,u_g) = (u_g + P_a - K_w)/F(n,S_w,u_g) \tag{25d}$$

$$F(n,S_w,u_g) = n\cdot\left\{ f'(S_w) - \frac{K_w}{S_w} - \frac{u_g + P_a}{1-S_w}\right\} \tag{25e}$$

Similarly, by eliminating both dS_w and du_w from Eqs.(8), (9) and (24) and by considering Eqs.(11) and Eq.(13), the following equation is obtained :

$$\mathrm{d}u_g = A_2(n,S_w,u_g)\cdot m_g + B_2(n,S_w,u_g)\cdot m_w + C_2(n,S_w,u_g)\cdot \mathrm{d}\varepsilon_v \tag{26a}$$

where,

$$A_2(n,S_w,u_g) = \frac{u_g + P_a}{1-S_w}\cdot\left(\frac{K_w}{S_w} - f'(S_w)\right)/F(n,S_w,u_g) \tag{26b}$$

$$B_2(n,S_w,u_g) = \frac{u_g + P_a}{1-S_w}\cdot\frac{K_w}{S_w}/F(n,S_w,u_g) \tag{26c}$$

$$C_2(n,S_w,u_g) = \left\{ f'(S_w) - \frac{K_w}{1-S_w} - \frac{K_w}{S_w}\right\}\cdot\frac{u_g + P_a}{F(n,S_w,u_g)} \tag{26d}$$

According to Bishop's equation [3], pore fluid pressure of unsaturated soils is expressed as follows :

$$u = u_g - \chi(S_w)\cdot(u_g - u_w) \tag{27}$$

Thus, pore fluid pressure increment du is expressed as follows :

$$\mathrm{d}u = \mathrm{d}u_g - \{f(S_w)\cdot\chi'(S_w) - f'(S_w)\cdot\chi(S_w)\}\cdot \mathrm{d}S_w \tag{28}$$

Table 1 Test cases of the gas migration test

Case No.	Dry Density (Mg/m^3)	Specimen Size		Measured values	
		Diameter (mm)	Height (mm)	Swelling pressure (MPa)	Hydraulic coductivity (m/s)
No.1	1.218	60	20	0.390	7.08×10^{-13}
No.2	1.202	60	20	0.391	7.25×10^{-13}
No.3	1.407	60	20	0.698	3.70×10^{-13}
No.4	1.392	60	20	0.637	3.79×10^{-13}
No.5	1.585	60	20	1.733	1.43×10^{-13}
No.6	1.607	60	20	1.854	1.40×10^{-13}
No.7	1.423	200	20	0.720	3.71×10^{-13}
No.8	1.391	200	20	0.639	4.29×10^{-13}

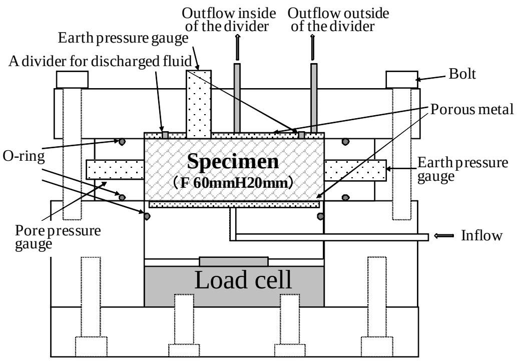

Fig.3 Sections of specimen cells used for the gas migration test from Case No.1 to CaseNo.6

Summary of equations describing gas migration phenomenon

Basic equations for the numerical analysis are Eqs. (8), (14) and (17). Figure 2 shows a procedure for calculating gas migration problem for one finite element using equations mentioned previously. Though Fig.2 shows a procedure if the strain increment of the element is given, it is possible to solve the problem similarly if the stress increment of the element is given.

OUTLINE OF GAS MIGRATION TEST FOR SIMULATION ANALYSIS

Outline of the gas migration test is described herein. Detailed description of the test is available in the literature 1.

Test conditions

Table 1 shows test cases of the gas migration test conducted in this study. In the test cases from No.1 to No.6, the effect of dry density of the specimen on the gas migration characteristics is investigated, while the effect of diameter of the specimen on the gas migration characteristics are

Table 2 Properties Bentonites used in this study

Type	Sodium bentonite
Specific gravity of soil particle	2.78 (Mg/m^3)
Montmorillonite content Note1)	50 (%)
Cation exchange capacity Note2)	1.040 (mequiv./g)
Capacity of exchangeable Na ion Note3)	0.611 (mequiv./g)
Capacity of exchangeable Ca ion Note3)	0.389 (mequiv./g)
Capacity of exchangeable K ion Note3)	0.024 (mequiv./g)
Capacity of exchangeable Mg ion Note3)	0.015 (mequiv./g)

Note1) Estimated by amount of absorption of methylene blue
Note2) The sum total of excahangeable Na ion, Ca ion, K ion and Mg ion capacity
Note3) Estimated by extraction using 1N-CH_3COONH_4

investigated comparing the results of test cases No.7 and No.8 with those of test cases No.3 and No.4. In this study, numerical simulation analysis is conducted for the Test Cases No.3 and No.5 in Table 1.

Fig.3 shows a cross section of an experimental cell which is used for the Test Cases from No.1 to No.6. Volume of discharged water and gas can be measured by porous metal which is divided into two pieces by a divider to allow volume of discharged water and gas near the inner wall of the vessel to be measured. Axial stress is measured by both a load cell and an earth pressure gauge, while radial stress and pore fluid pressure are measured by three earth pressure gauges and a pore pressure gauge respectively. Table 2 shows basic properties of bentonite used in this study. Helium gas instead of hydrogen gas is used for the tests.

Water infiltrated into the specimen one-dimensionally for complete water saturation of the specimen. At the end of infiltration, hydraulic conductivity written in Table 1 is measured. After exchanging the lower wet porous metal for a dry porous metal, air pressure of 0.3 MPa, water pressure of 0.3 MPa are applied as back pressure to lower end of the specimen, upper end of the specimen, respectively. This state of stresses is called initial state in this paper. Gas migration tests start from the initial state. Swelling pressure at the initial state is written in Table 1.

Test results

Fig. 4 shows results of the Test Case No.3, showing change of gas pressure, earth pressure, pore fluid pressure,

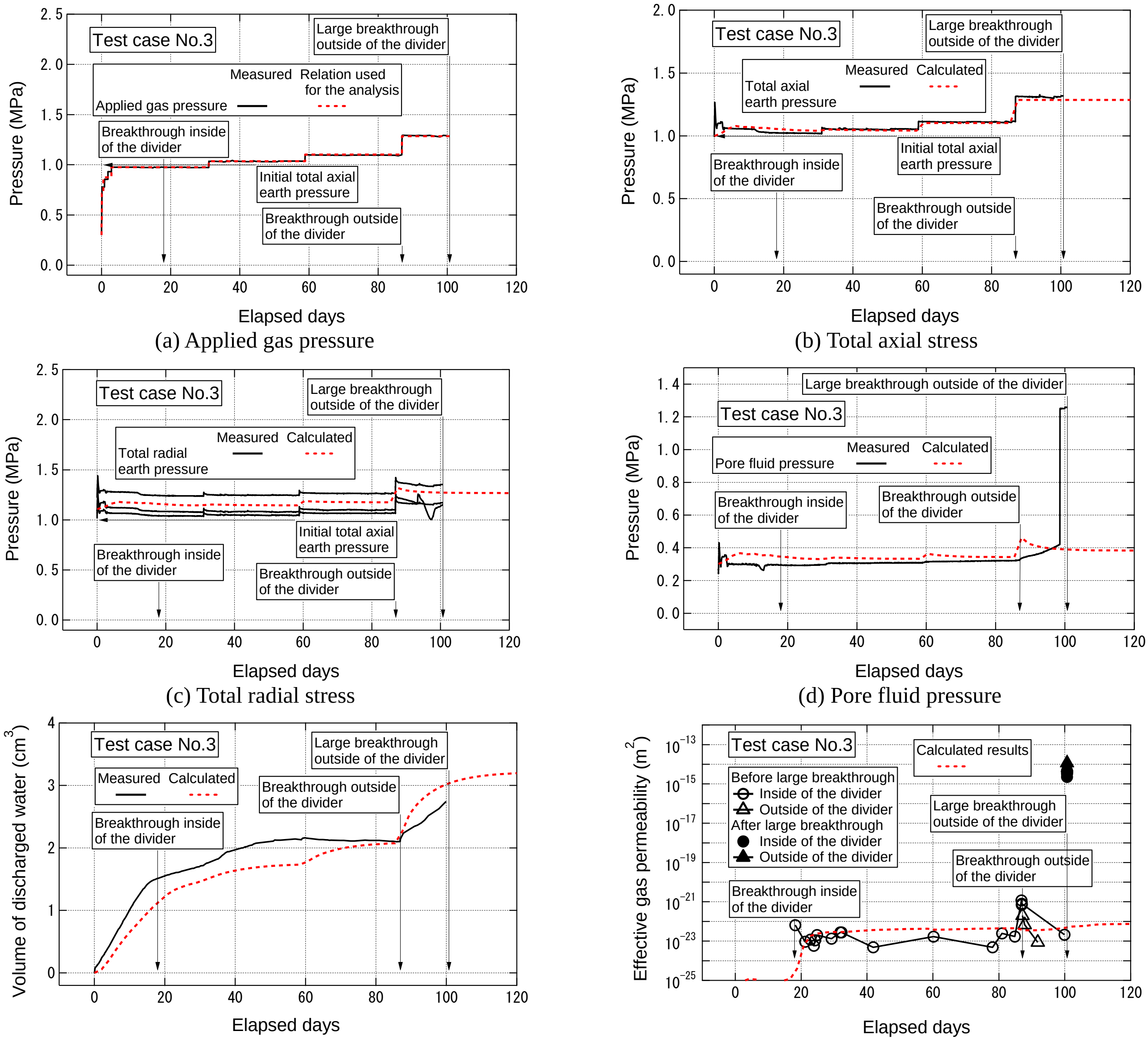

(a) Applied gas pressure

(b) Total axial stress

(c) Total radial stress

(d) Pore fluid pressure

(e) Volume of discharged water

(f) Effective gas permeability

Fig.4 Measured results and calculated results with the passage of time (Test case No.3)

volume of discharged water and effective gas permeability with the passage of time. Breakthrough of gas migration, which defined as first appearance of small bubbles in the semitransparent drainage tube out from the specimen, occurs when applied gas pressure is equal to the initial total axial stress. By increasing the gas pressure more, large breakthrough of gas migration, which defined as a sudden and sharp increase of amount of discharged gas, occurs. When the total gas pressure exceeds the initial total axial stress, the total axial stress is always equal to the total gas pressure because specimens shrink in the axial direction with causing clearance between the lower end of the specimen and the lower porous metal as illustrated in Fig.5.

Effective gas permeability, which is defined by Eq.(29), after the large breakthrough is ranging from 10^8 to 10^{10} times larger than that measured before the large breakthrough of gas migration as shown in Fig.4(f).

$$K_{g,eff} = \frac{Q\mu HP_1}{A}\cdot\frac{2}{\{P_{in}(t)\}^2-\{P_{out}\}^2} \tag{29}$$

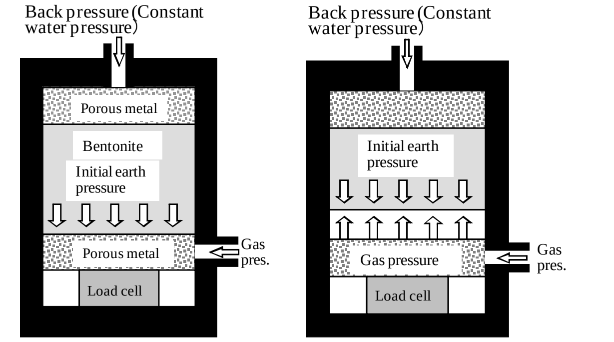

(a) Gas pres.<Initial total pres. (b) Gas pres.>Initial total pres.

Fig.5 Shrinkage of specimen due to gas pressure over initial axial total stress

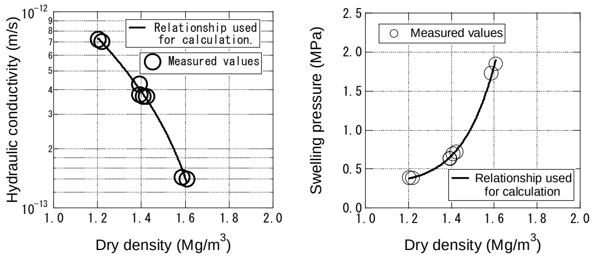

Fig.6 Hydraulic conductivity and swelling pressure of saturated bentonite and their relation to dry density

where, $K_{g,eff}$: effective gas permeability, Q : flow rate of gas in a normal state (Nm^3/s), μ : coefficient of viscosity, P_{in} : inflow gas pressure (Pa), P_{out} : outflow gas pressure (Pa), A : area of radial section of the specimen (m^2), H : height of the specimen (m), P_1 : atmospheric pressure

This fact means that the large breakthrough of gas migration is effective in reducing gas pressure accumulated in the vault for radioactive waste disposal and that the large breakthrough must be accompanied by the damage , such as fissures, to the specimen.

SIMULATION ANALYSIS

Determination of parameters concerning properties of bentonite

a) Hydraulic conductivity and swelling pressure of fully saturated bentonite

Fig. 6 shows relations between hydraulic conductivity and dry density, and between swelling pressure and dry density. For numerical simulation analysis, solid lines in Fig. 6 are used.

b) Young's modulus and Poison's ratio of fully saturated bentonite under drained condition

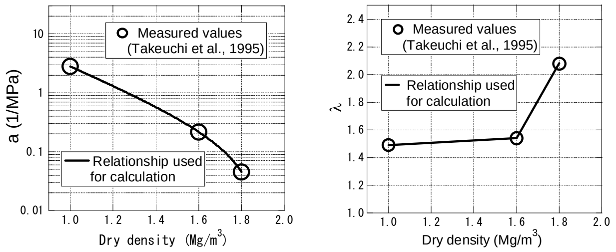

Fig.7 Relationship between van Genughten's parameters and dry density

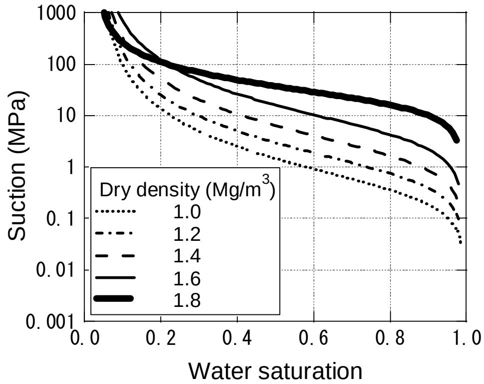

Fig.8 Relationship between suction and water saturation

Coefficient of volume compressibility m_v in the one-dimensional consolidation theory, is calculated by the following equation [1] :

$$m_v = -(d\rho_{db}/\rho_{db})/dP_s = -(d\rho_{db}/dP_s/\rho_{db}) \tag{30}$$

where, ρ_{db} : dry density of bentonite, P_s : swelling pressure

Further, Young's modulus can be calculated as follows :

$$E_d = (1+\nu_d)\cdot(1-2\nu_d)/\{(1-\nu_d)\cdot m_v\} \tag{31}$$

c) Relations between suction and water saturation

The relationship between effective water saturation S_e and water saturation S_w is expressed as follows :

$$S_e = \{S_w \cdot e/(1+e) - \theta_r\}/(\theta_{sat} - \theta_r) \tag{32}$$

where, θ_r : minimum volume water content, θ_{sat} : saturated volume water content

Further, the relationship between effective water saturation S_e and suction u_c is expressed by van Genughten's model [4] as follows :

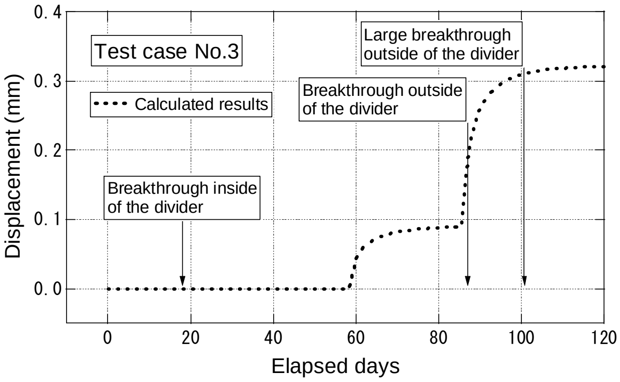

Fig.9 A calculated result of axial displacement of lower end of the specimen

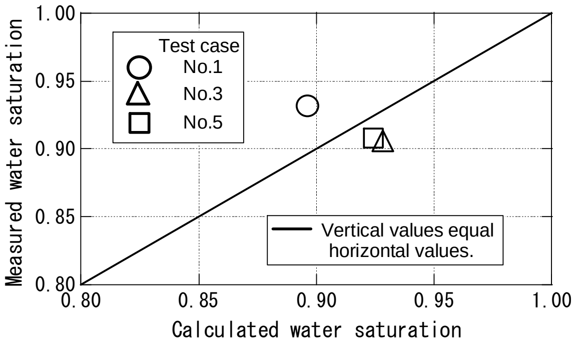

Fig.10 Comparison between calculated results and measured results on water saturation of the specimen after large breakthrough

$$u_c = 1/a \cdot \left\{ (S_e)^{\frac{\lambda}{1-\lambda}} - 1 \right\}^{\frac{1}{\lambda}} \quad (33)$$

where, a, λ : constants which are independent of effective water saturation S_e

Based on the results of tests by Takeuchi et al. [5], the relationship between the constants in Eq.(33) of KunigelV1 and dry density is shown in Fig.7. Figure 8 shows the relationship between suction and water saturation calculated by Eq.(33) using the constants evaluated by Fig.7

e) Relationship between bulk modulus and water saturation

The relationship between bulk modulus and water saturation is expressed based on the empirical relation obtained by Takaji and Suzuki [6]. The relationship is shown as follows :

$$\begin{aligned} K_d(S_w) - K_{d,sat} &= (E_{50} - E_{50,sat}) / \{3 \cdot (1 - 2\nu_d)\} \\ &= (1 - S_w) / \{3 \cdot (1 - 2\nu_d)\} \cdot (-\partial E_{50} / \partial S_w) \end{aligned} \quad (34)$$

where, $K_d(S_w)$, $K_{d,sat}$: bulk modulus of soil at water saturation of S_w, water saturated bulk modulus, respectively, E_{50}, $E_{50,sat}$: secant Young's modulus of soil at water saturation of S_w, secant Young's modulus of saturated soil, respectively

f) K_{dr0} in Eq.(18b)

By integrating Eq.(18a) on the condition that $d\varepsilon_v$ in Eq.(18a) equals zero, swelling pressure affected by initial water saturation can be calculated. Further, by comparing the calculated results with swelling pressure test results, K_{dr0} is determined.

g) χ in Eq.(27)

Based on the pore fluid pressure, applied gas pressure and water pressure as back pressure during the gas migration test, χ in Eq.(27) is determined as follows :

$$\chi(S_w) = S_w \quad (35)$$

h) Relationship between relative hydraulic conductivity and water saturation

van Genughten's model is adopted for the relationship between relative hydraulic conductivity and water saturation. In that case, the parameter λ in the equation is determined the relationship in the right-hand side of Fig.7.

$$k_{wr} = (S_e)^{1/2} \cdot \left[1 - \left\{ 1 - (S_e)^{\frac{\lambda}{\lambda-1}} \right\}^{\frac{\lambda-1}{\lambda}} \right]^2 \quad (36)$$

i) Relationship between relative gas permeability and water satulation

The relationship between relative gas permeability k_{gr} and water saturation S_w is reportedly expressed by Corey's model as follows [7] :

$$k_{gr} = (1 - S_e)^2 \cdot \left\{ 1 - (S_e)^{\frac{2+n_g}{n_g}} \right\} \quad (37)$$

where, n_g : a constant which is independent of effective water saturation S_e

Calculated results by Corey's model of n_g=2.08 coinside well with measured results by Tanai et al [6]. However, in that case, k_{gr}=0 if S_w is more than 0.8. This contradicts most of results of gas migration tests.

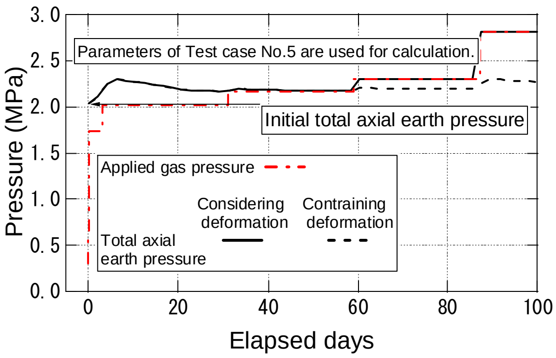

(a) Total axial stress

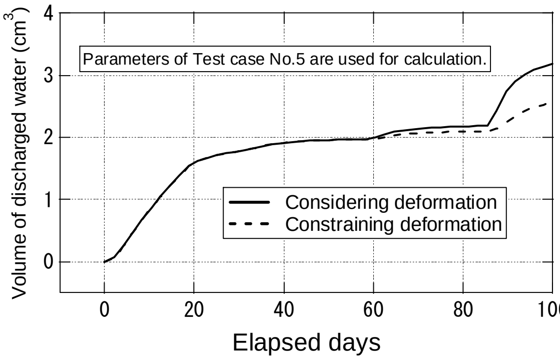

(b) Volume of discharged water

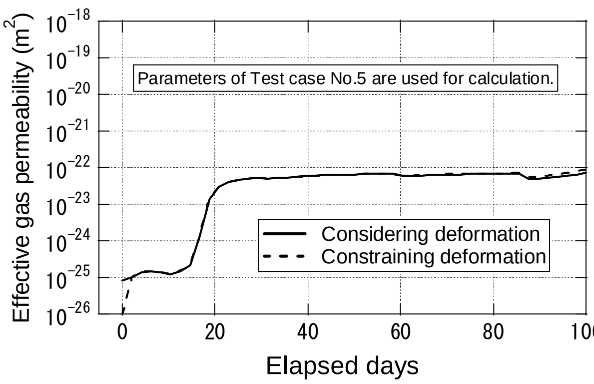

(c) Effective gas permeability

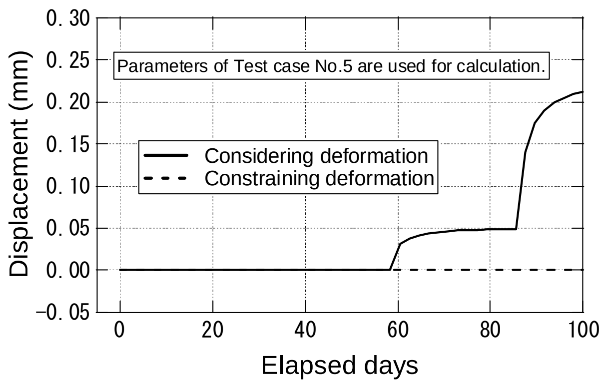

(d) Axial displacement

Fig.11 Effect of constraint of deformation of elements on calculated results

Therefore, if S_w is more than 0.8, k_{gr} is calculated by the following equation :

$$a_{gr} = k_{gr} / (1 - S_w) \qquad (38)$$

0.05 is adopted for the value of a_{gr} in Eq.(38) based on the theoretical consideration on the results of the gas migration test

Comparison between measured results and calculated results

Figure 4 shows calculated results with measured results. As for axial total stresses in Fig.4(b), radial total stress in Fig.4(c) and pore fluid pressure in Fig.4(d), measured results can be simulated by the calculated results with accuracy.

Figure 4(e) shows volume of discharged water with the passage of time. Before the large breakthrough, the measured result can be simulated with accuracy by the numerical analysis.

Figure 4(f) shows effective gas permeability with the passage of time. As shown in Fig.4(f), calculated effective gas permeability coincides with measured effective gas permeability with accuracy before the large breakthrough. Though, as mentioned previously, effective gas permeability after the large breakthrough is ranging from 10^8 to 10^{10} times larger than that measured before the large breakthrough, the calculated results can not simulate the behavior. This is merely because sudden increase in effective gas permeability due to damage to the specimen is not considered in this numerical analysis code. This is desirable to be improved.

Figure 10 shows comparison between calculated results and measured results in terms of water saturation of specimens after large breakthrough. Calculated results in Fig.10 are calculated from volume of discharged water at large breakthrough. Figure 10 shows good coincidence between calculated results and measured results.

As described previously, by increasing applied gas pressure beyond initial axial total stress, the specimen shrink in axial direction with causing clearance between the lower end of the specimen and the lower porous metal as illustrated in Fig.5. In order to simulate this behavior, a joint element is placed between the lower end of the specimen and the lower porous metal. Consequently, as shown in Fig.9, displacement of the lower end of the specimen can be expressed.

As described above, the gas migration test results can be simulated by the proposed numerical analysis method with accuracy.

The effect of constraining deformation of soil on the calculated results by the proposed numerical method

Calculation without considering deformation of soil is conducted by constraining deformation of each element in the one-dimensional gas migration analysis to compare with the calculated results of considering deformation. Both calculated results are shown in Fig.11. At the same time, shrinkage of the specimen begins at about 60 elapsed days from the beginning of pressurization as shown in Fig.11(d), difference between both calculated results can be seen in Figs.11(a) and Fig.11(b). After about 60 elapsed days, total axial stress together with volume of discharged water of constraining deformation condition are smaller than those calculated results of considering deformation. This difference is attributable to shrinkage of the specimen. Contrastively, calculated effective gas permeability is almost not affected whether deformation of the soil elements is constrained or not.

Therefore, it is revealed that accuracy of the calculated results is possibly enhanced by considering deformation of soil during pressurization.

CONCLUSIONS

In this study, a method for simulating gas migration through the compacted bentonite is proposed. The proposed method can analyze coupled hydrological-mechanical processes using the model of two-phase flow through deformable porous media.

Validity of the proposed analytical method is examined by comparing gas migration test results with the calculated results. It is revealed that the proposed method can simulate gas migration behavior through compacted bentonite with accuracy.

The effect of constraining deformation of soil on the calculated results is investigated. Calculation without considering deformation of soil is conducted by constraining deformation of each element in the one-dimensional gas migration analysis to compare with the calculated results. As a result, it is revealed that accuracy of the calculated results is possibly enhanced by considering deformation of soil during pressurization.

ACKNOWLEDGMENTS

This study was conducted by the request of The Federation of Electric Power Companies of Japan. The authors are grateful to all the persons who gave assistance to this study. Especially, the author is grateful to Dr. Sato (Goscience research laboratory Co, Ltd.) for making and running the computer program of the method described in this paper.

REFERENCES

[1] Tanaka, Y., Hironaga, M. and Kudo, K., 2010, “Gas migration mechanism of saturated dense bentonite and its modeling, ” Proc. of ICEM-2010, Paper No. ICEM2010-40011.

[2] For example, Mori, K., Tada, K., Tasaka, H., Okamoto, S. and Fujiwara, A., 2005, A discussion of the applicability of water/air two-phase flow modeling to in-situ gas migration behavior in engineered barrier system, Proc. of the 34 th Symposium on Rock Mechanics, pp.41 - 48. (in Japanese)

[3] Bishop, A.W. and Blight, G. E., 1963, “Some Aspects of Effective Stress in Saturated and Unsaturated Soils,” *Geotechnique*, **13**(**3**), pp.177－197.

[4] Van Genughten, M.T., 1980, “A Closed-Form Equation for Predicting the Hydraulic Conductivity of Unsaturated Soils,” Journal of Soil Science Society America, Vol.44, pp.892-898.

[5] Takeuchi,S., Hara,K. and Nakano,M., 1995, “Water retention curve, water diffusivity and water movement of compacted bentonite,” *Soils and Foundations*, **35**(**3**), pp.129-137, (in Japanese).

[6] Takaji, K. and Suzuki, H., 1999, Static mechanical properties of buffer material (Research Report), JNC Tokai-jigyousyo, JNC TN8400 99-041. (in Japanese)

[7] Tanai, K., Sato, H., Murakami, T. and Inoue, M., 1999, A preliminary assessment of gas diffusion and migration (Research Report), JNC Tokai-jigyousyo, JNC TN8400 99-045. (in Japanese)

G.3：Poster－Gas Migration Mechanism of Saturated Highly-compacted Bentonite and its Modelling)

Gas Migration Mechanism of Saturated Highly-compacted Bentonite and its Modelling

Central Research Institute of Electric Power Industry
Yukihisa Tanaka, Michihiko Hironaga, Kohji Kudo

Introduction : In the current concept of repository for radioactive waste disposal, compacted bentonite will be used as an engineered barrier mainly for inhibiting migration of radioactive nuclides. Hydrogen gas can be generated inside the engineered barrier by anaerobic corrosion of metals used for containers, etc. If the gas generation rate exceeds the diffusion rate of dissolved gas inside of the engineered barrier, gas will accumulate in the void space inside of the engineered barrier until its pressure becomes large enough for it to enter the bentonite as a discrete gaseous phase. It is expected to be not easy for gas to entering into the bentonite as a discrete gaseous phase because the pore of compacted bentonite is so minute. Therefore it is necessary to investigate the following subjects:

a) Effect of the accumulated gas pressure on surrounding objects such as concrete lining, rock mass.
b) Effect of gas breakthrough on the barrier function of bentonite.
c) Revealing and modeling gas migration mechanism for evaluating the scale effects in laboratory specimen test.

Therefore in this study, firstly, gas migration tests for saturated highly compacted bentonite are conducted to investigate and to model the mechanism of gas migration phenomenon. Secondly, a method for evaluating gas pressure of large gas breakthrough, which is defined as a sudden and sharp increase in gas flow rate out of the specimen, is proposed. Finally, a finite element code for simulating gas migration in compacted bentonite based on the model of two-phase flow through deformable porous media is newly developed.

1. Gas Migration Mechanism of Saturated Highly-compacted Bentonite

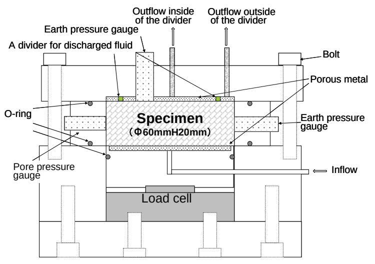

Axial sectional view of the vessel for the test

Properties Bentonite used in this study

Name	KunigelV1
	Sodium bentonite
Producing district	Tsukinuno inYamagata Pref., JAPAN
Density of clay particle (Mg/m^3)	2.78
Montmorillonite content (%)	50
Cation exchange capacity (meq/g)	1.040
Capacity of exchangeable Na ion (meq/g)	0.611
Capacity of exchangeable Ca ion (meq/g)	0.389
Capacity of exchangeable K ion (meq/g)	0.024
Capacity of exchangeable Mg ion (meq/g)	0.015

Test cases of Gas migration test by CRIEPI

Case No.	Dry Density (Mg/m^3)	Specimen Size: Diameter (mm)	Specimen Size: Height (mm)	Measured values: Swelling pressure (MPa)	Measured values: Hydraulic coductivity (m/s)
No.1	1.218	60	20	0.390	7.08×10^{-13}
No.2	1.202	60	20	0.391	7.25×10^{-13}
No.3	1.407	60	20	0.698	3.70×10^{-13}
No.4	1.392	60	20	0.637	3.79×10^{-13}
No.5	1.585	60	20	1.733	1.43×10^{-13}
No.6	1.607	60	20	1.854	1.40×10^{-13}
No.7	1.423	200	20	0.720	3.71×10^{-13}
No.8	1.391	200	20	0.639	4.29×10^{-13}

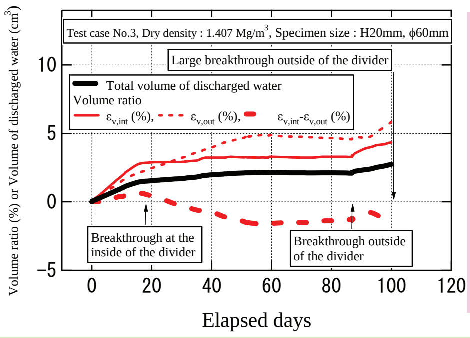

Definition of Volume Ratio
$\varepsilon_{v,int}$: volume of discharged water inside the divider divided by soil volume inside the divider.
$\varepsilon_{v,iout}$: volume of discharged water outside of the divider divided by soil volume outside of the divider.

Time history of volume of discharged water

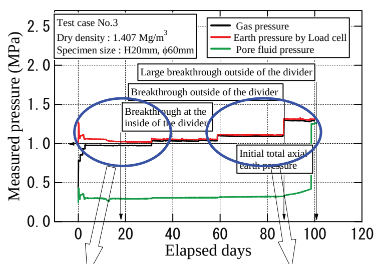

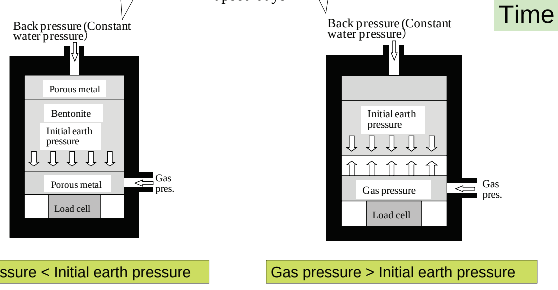

Constriction of specimen due to gas pressure over initial earth pressure

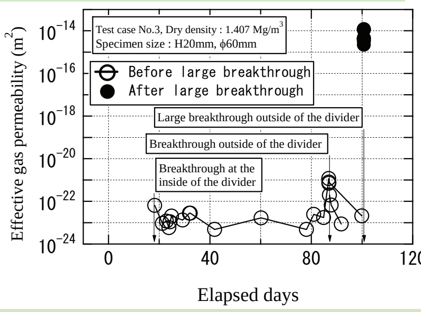

Time history of effective gas permeability

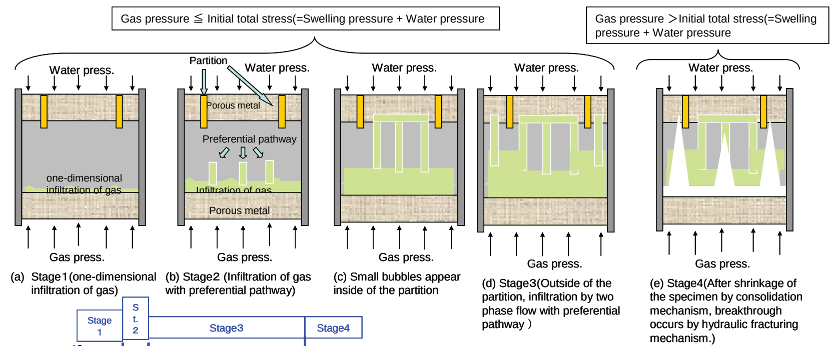

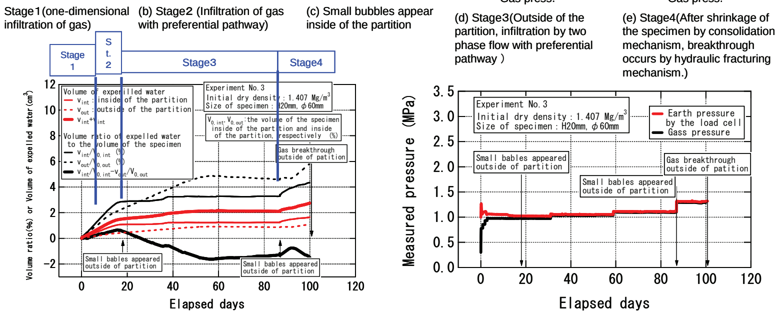

Estimated gas migration mechanism from the beginning of gas pressurization to large breakthrough

2. Modelling Large breakthrough

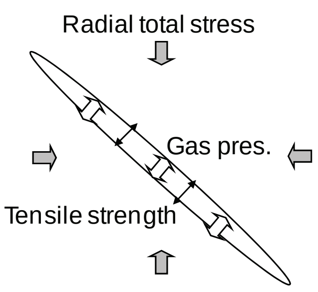

(a) a section perpendicular to the forward direction of the fissure

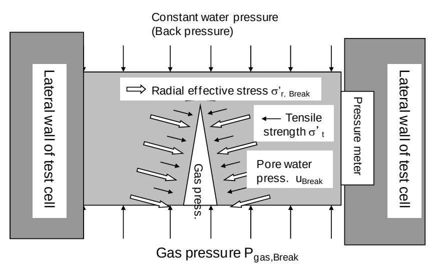

(b) a section parallel to the forward direction of the fissure

Stress state in the specimen at large breakthrough assuming hydraulic fracturing mechanism

Hydraulic Fracturing Criteria

$$P_{gas} \geq \sigma'_r + u + \sigma'_t$$

P_{gas} :gas pressure
σ'_t :tensile strength
σ'_r :effective radial stress
u :pore water pressure

Pore water pressure u and effective radial stress σ'_r are evaluated using one-dimensional consolidation theory assuming earth pressure coefficient K_0 is 0.5.

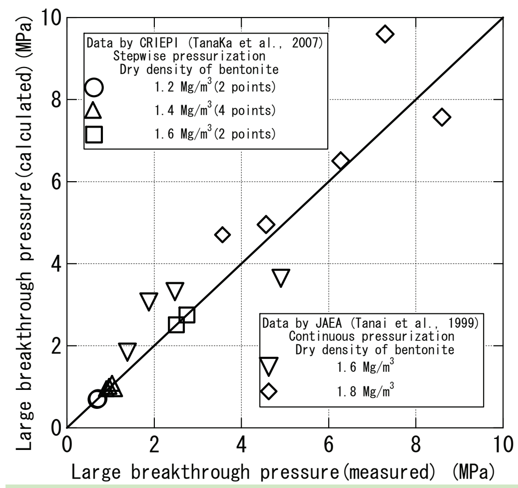

Comparison between measured results and calculated results by the proposed method

3. Modelling gas migration behaviour by Gas/Liquid Two-phase Flow through Deformable Porous Media

Basic assumptions of CRIEPI's Code

A finite element code for simulating gas migration in compacted bentonite by CRIEPI

Basic model
The model of two-phase flow through deformable porous media

Basic equations
·continuity of gas flow,
·continuity of water flow,
·stress-strain relationship of soil
·equilibrium of forces

Comparison between measured results calculated results by the CRIEPI's code.

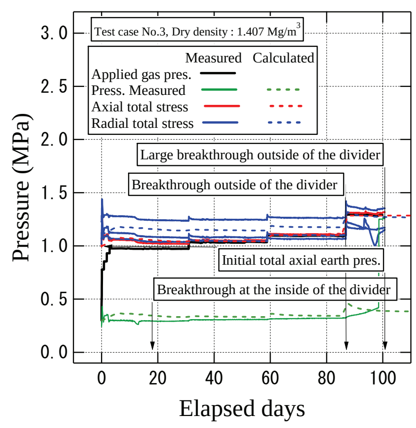

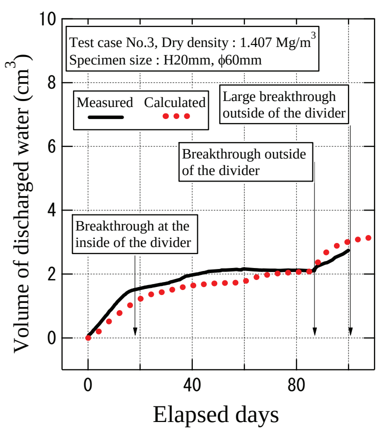

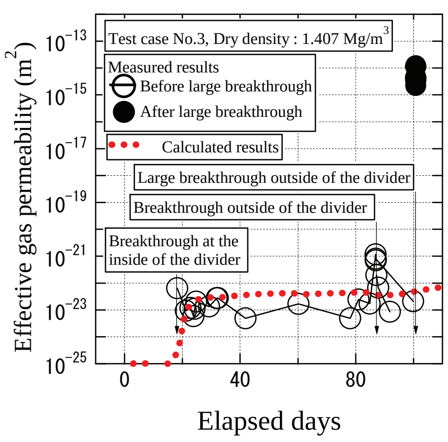

Calculated results by the CRIEPI's code.

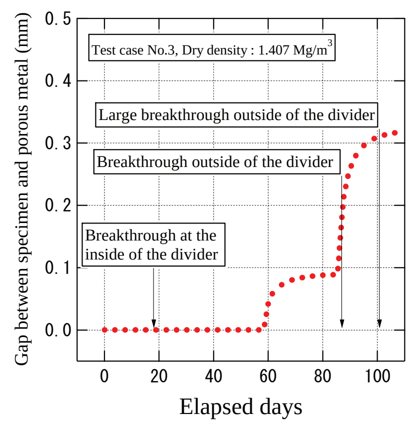

CONCLUSIONS

(1) Gas migration mechanism of saturated dense bentonite was clarified.

(2) Large breakthrough was modeled assuming hydraulic fracturing mechanism and one-dimensional theory. The calculated results showed good agreement with experimental results.

(3) A finite element code for simulating gas migration in compacted bentonite based on the model of two-phase flow through deformable porous media was newly developed by CRIEPI.

(4) It was revealed that the results of the gas migration test can be simulated by the newly developed finite element code.

H：横須賀計畫

H.1 Slides－Introducttion of Yokosuka project

Nov. 26, 2012

Edited based on CRIEPI Report N15 andN11038

NUMO-CRIEPI Joint Research

Yokosuka D&V Project

Introduction of Yokosuka project:

- Typical results of validation of survey technology for siting program for HLW -

- Borehole survey (and geophysical prospecting) technology (FY 2006-2010)
- Ground water monitoring technology (FY 2010-2011)

Three Stages of Site Selection Program by NUMO

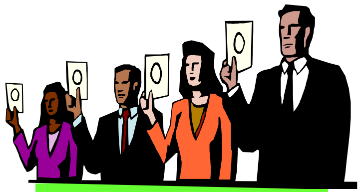

Volunteers

Preliminary Investigation Areas (PIAs)

Detailed Investigation Areas (DIAs)

Final Repository Site

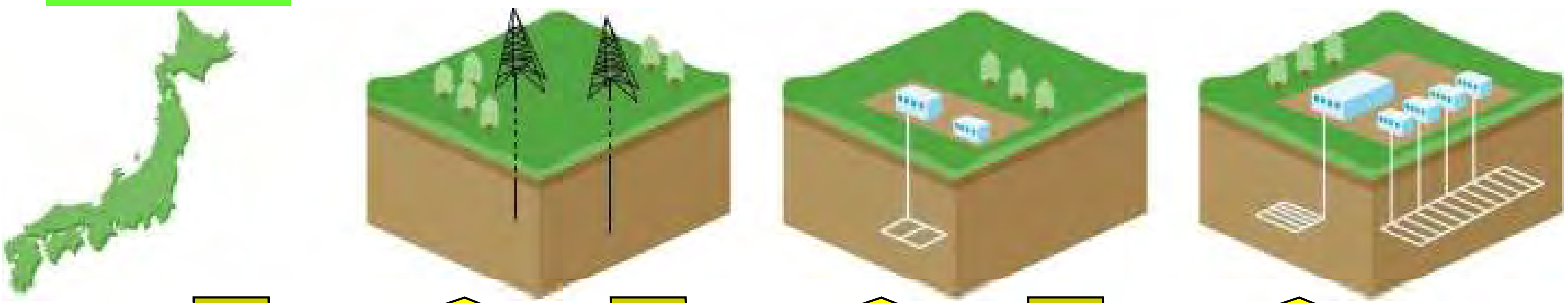

Selection of PIAs

Areas:
  Volunteer areas
  and their surroundings
Methods:
  Literature Surveys (LS)

Selection of DIAs

Areas: PIAs
Methods:
  Borehole survey,
  geophysical prospecting, etc.
  (**Preliminary Investigations**)

Selection of repository site

Areas: DIAs
Methods:
  Detailed surface explorations,
  measurements and tests in
  underground investigation facilities
  (Detailed Investigations)

Progress and present situation of Yokosuka Project

●Main objectives of Yokosuka Project in FY 2006-2010:

➢To confirm the **applicability of existing survey technology** for obtaining properties of geological environment in the stage of **Preliminary Investigation**.

➢**Key technologies:** (Yokosuka DV site: Neogene sedimentary and coastal environment)

•**Borehole survey**: applicability to various geological conditions (Miura Group/Hayama Group in YDP-1,2 borehole), and characterization of the properties of geological environment of these two Groups.

•**Geophysical prospecting**: validity of surface seismic and electromagnetic prospecting methods (for obtaining information about geological structure, and salt/fresh water boundary before borehole surveys)

Division of cooperative research	Main objectives of survey technologies	Main items of survey technologies	Research progress every fiscal year 2006	2007	2008	2009	2010	2011
Part 1 (2006-2007)	Technology for Preliminary Investigation	・Literature survey	■					
		・Surface survey (Geological and geophysical (electrical))	■					
		・Borehole survey (YDP-1) (Depth=350m, mainly Miura G.)	■	■				
Part 2 (2008-2009)		・Borehole survey (YDP-2) (Depth=500m, mainly Hayama G.)			■	■		
Part 3 (2010)		・Geophysical prospecting (Additional: seismic, electromagnetic)					■	
	Technology for groundwater monitoring	・Groundwater monitoring (Installation of MP55 for YDP-2)					■	
Part 4 (2011)		・Groundwater monitoring (Baseline assessment for groundwater)						■

Completed !! (Technology for Preliminary Investigation, 2006–2010)

Research progress of Yokosuka Project in FY 2006-2011

➡ A verification study of **monitoring technology** for obtaining **baseline data of groundwater** newly started in FY 2010 (pressure measurement still continued in 2012).

Outline of the Yokosuka Project in FY 2006-2010

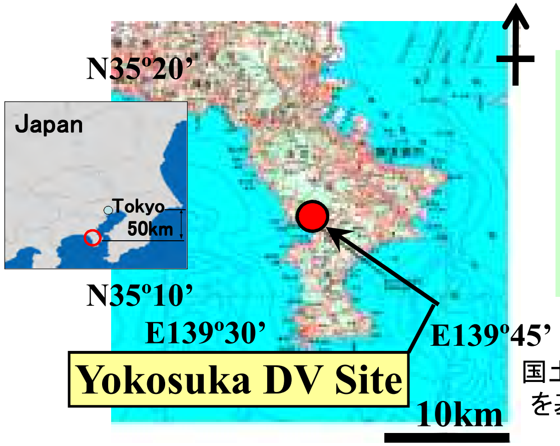

国土地理院（1997）
を基に編集・加筆

"Neogene sedimentary and coastal environment"

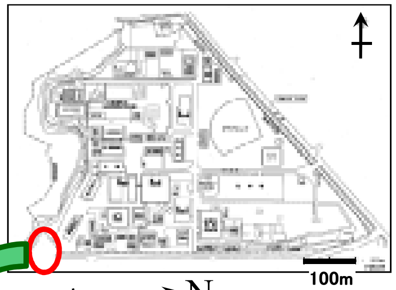

Survey area: CRIEPI Yokosuka grounds (A drilling yard is limited in only the SW corner)

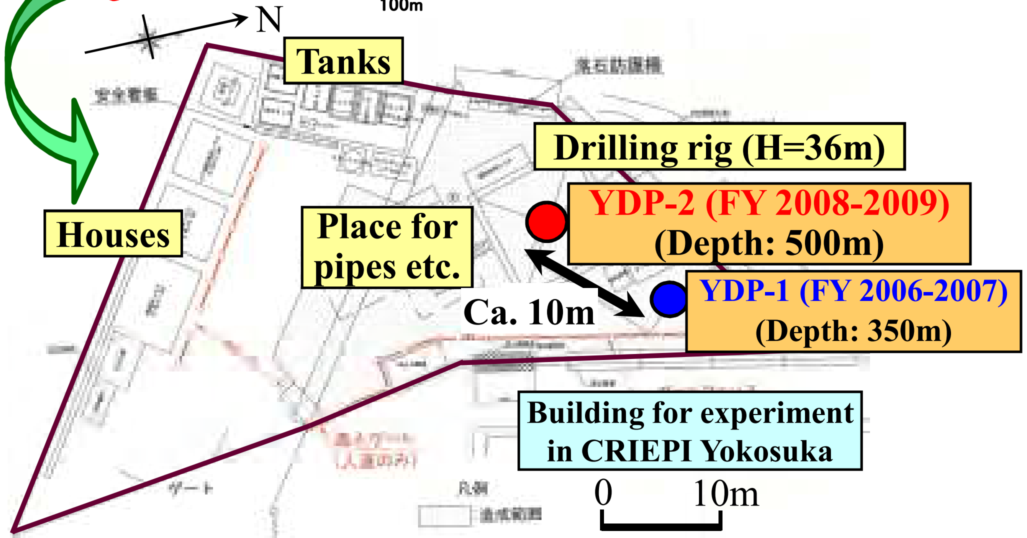

Drilling yard

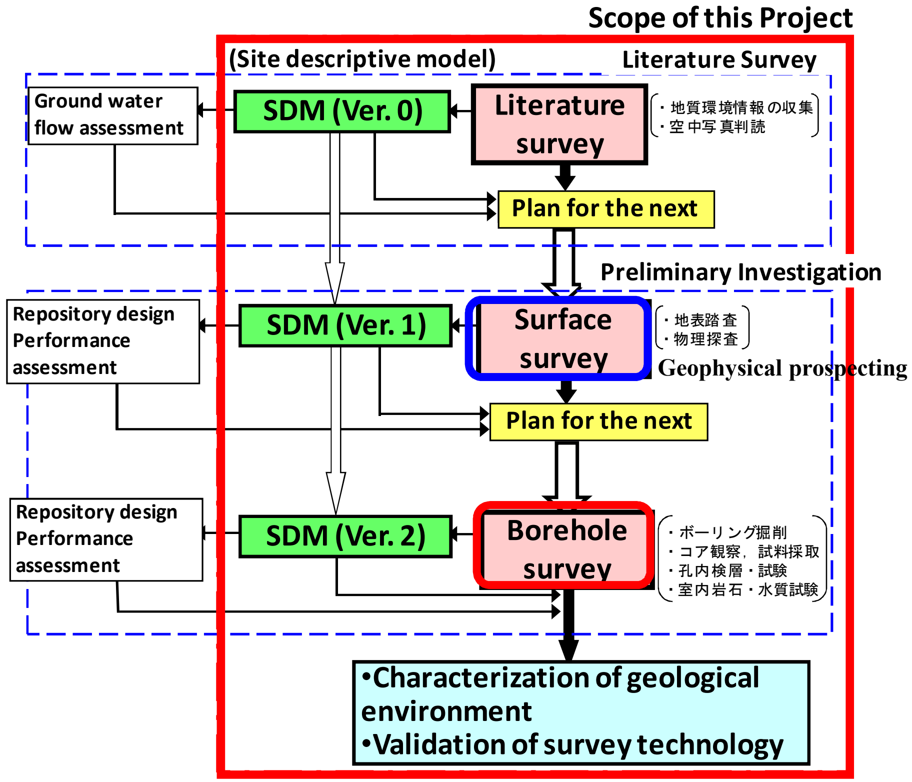

Investigation flow and the scope of Yokosuka Project in FY 2006-2010

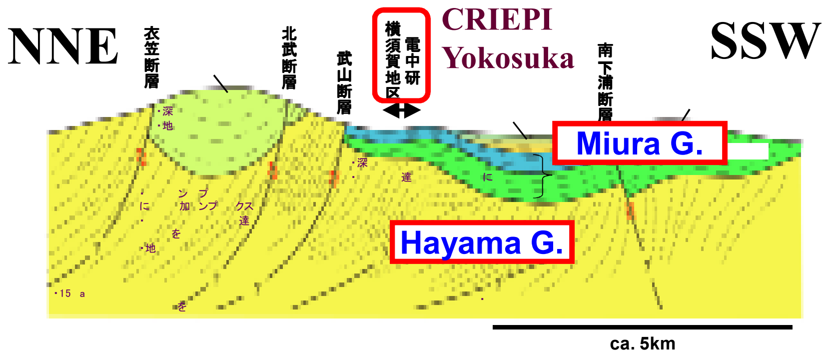

Conceptual model of geological structure

Revision of geological model due to the restriction of earlier surveys

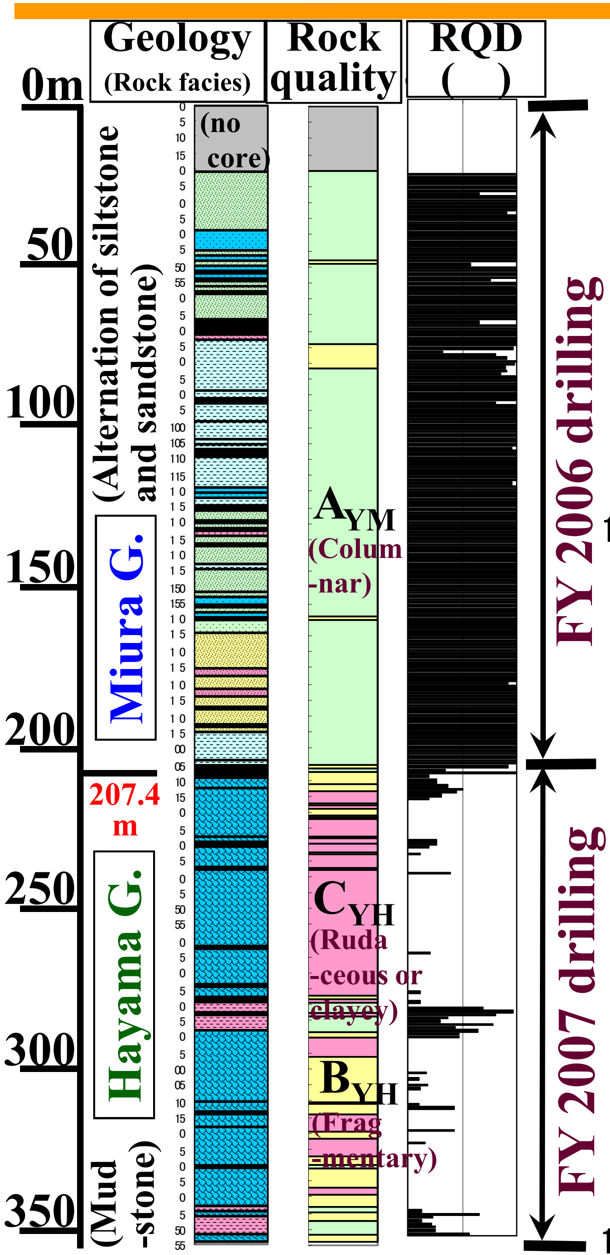

Results of core observation of YDP-1 (FY 2006-2007)

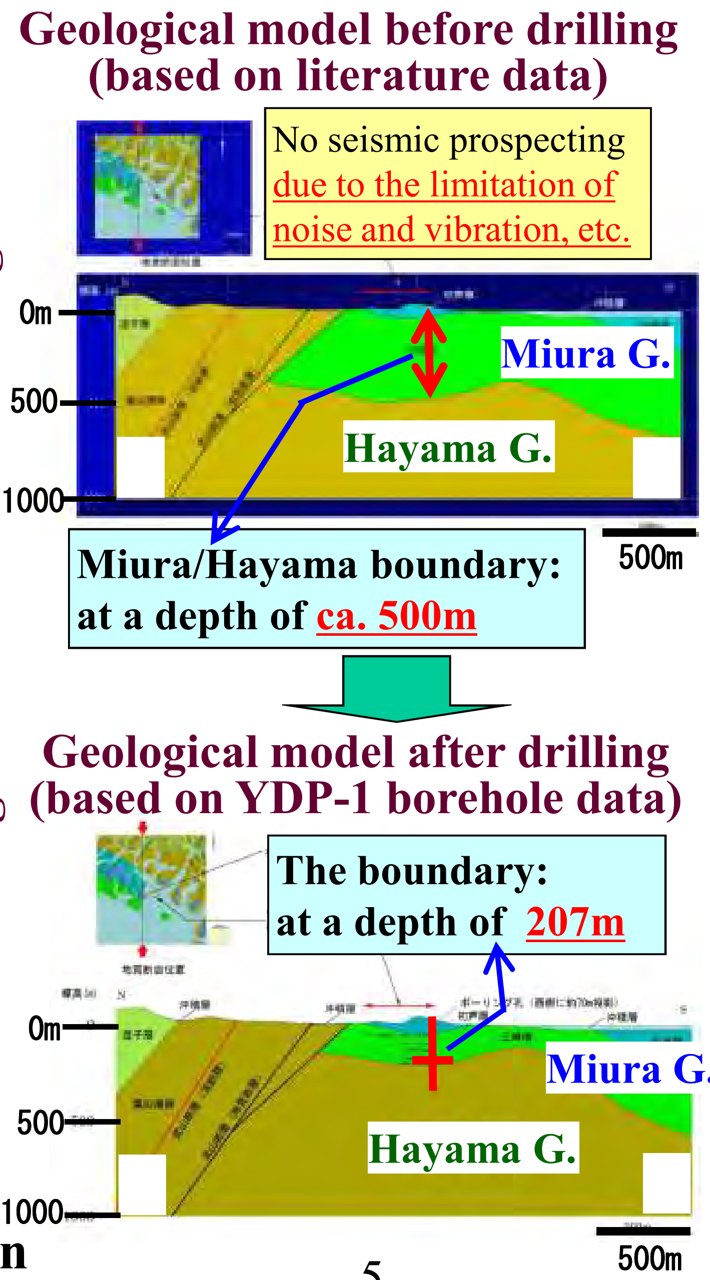

- The restriction of the surface survey stage (no seismic prospecting) caused a high degree of uncertainty of the determination of the Miura G./Hayama G. boundary.
- Such uncertainty should be reduced through surface seismic prospecting, if there is no restriction.

Under the restriction, microtremor array observation method (no artificial seismic source) was carried out after YDP-1 drilling and its validity was confirmed.

Confirmation of the Miura/Hayama boundary using microtremor array

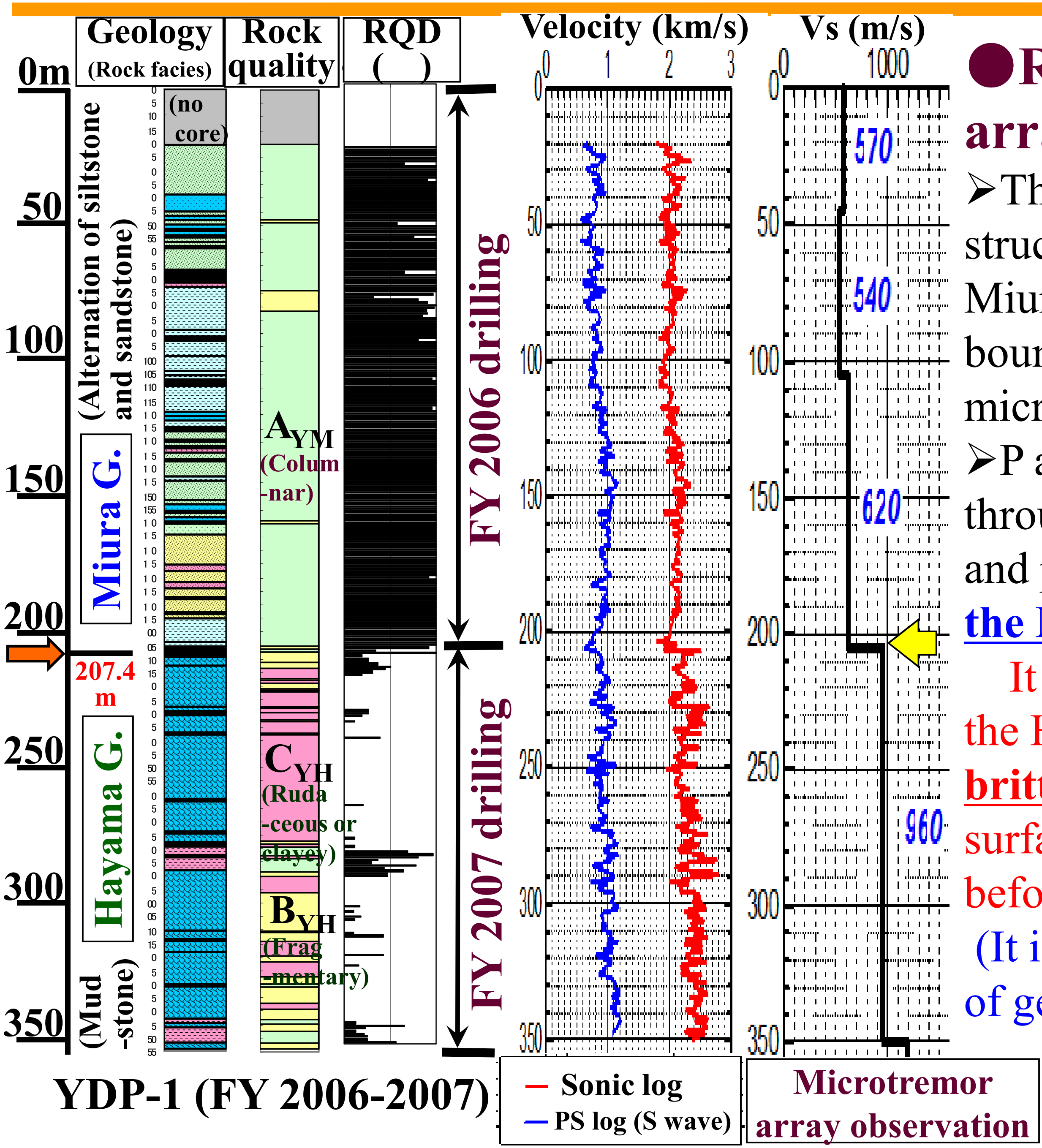

●Result of microtremor array observation method:

- The boundary of velocity structure (corresponding to the Miura/Hayama geological boundary) was detected using microtremor array observation.
- P and S wave velocity obtained through both geophysical logging and prospecting indicates:

the Miura G. < **the Hayama G.**

It seems difficult to recognize the Hayama G. as **fractured and brittle rock** through the results of surface geophysical prospecting before borehole survey.

(It is beyond the limits of ability of geophysical prospecting.)

Confirmation of the Miura/Hayama boundary using VSP after drilling

VSP was conducted after each of YDP-1 and YDP-2 drilling using a mini-vibrator in consideration of the effects of its noise and vibration.

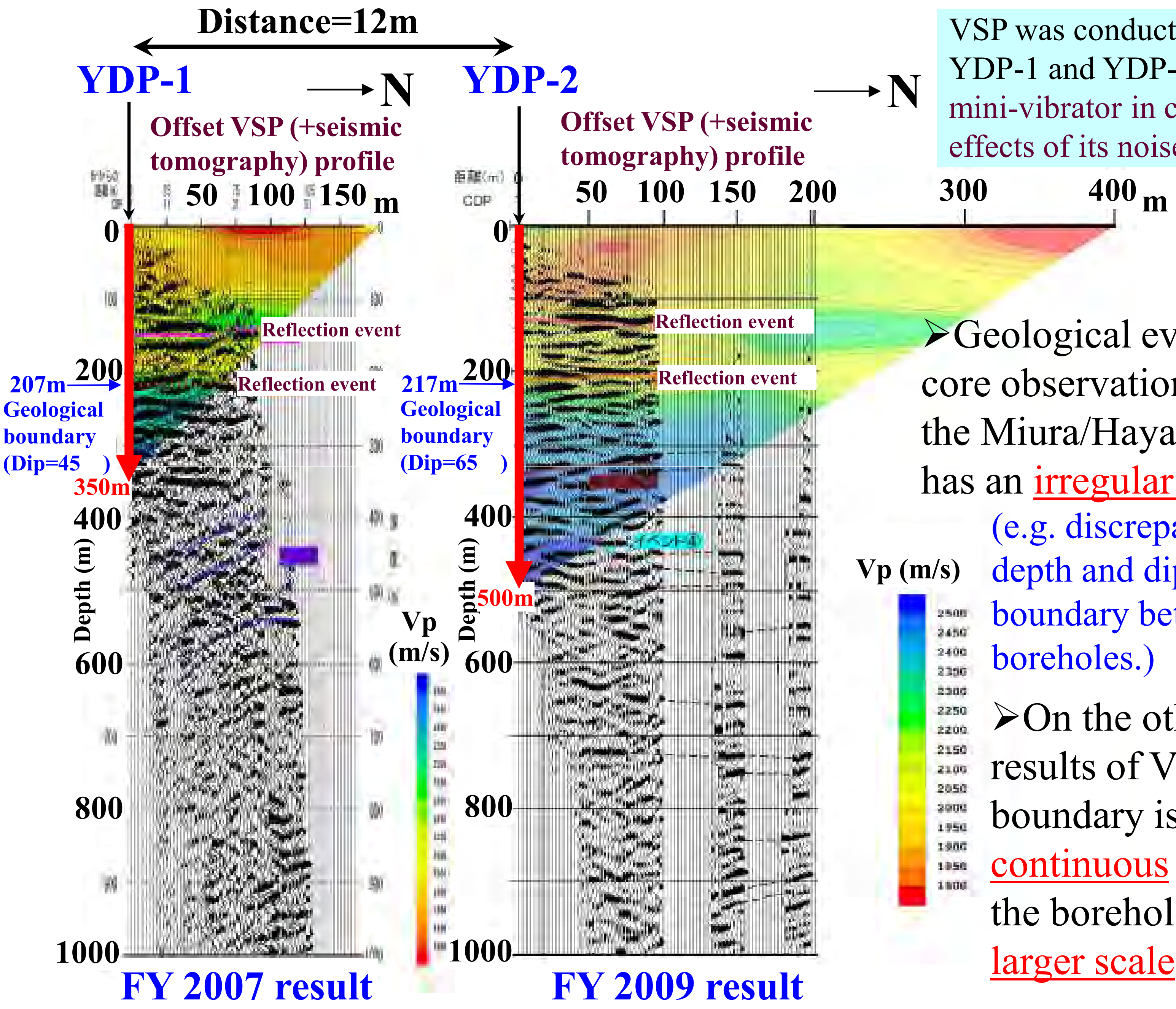

- ➢Geological evidence (from core observation) indicates that the Miura/Hayama boundary has an irregular shape locally.
  (e.g. discrepancy in encounter depth and dip angle of the boundary between the two boreholes.)
- ➢On the other hand, the results of VSP suggest the boundary is horizontally continuous around from the borehole point on a larger scale.

Correlation of Geology between YDP-1 and 2

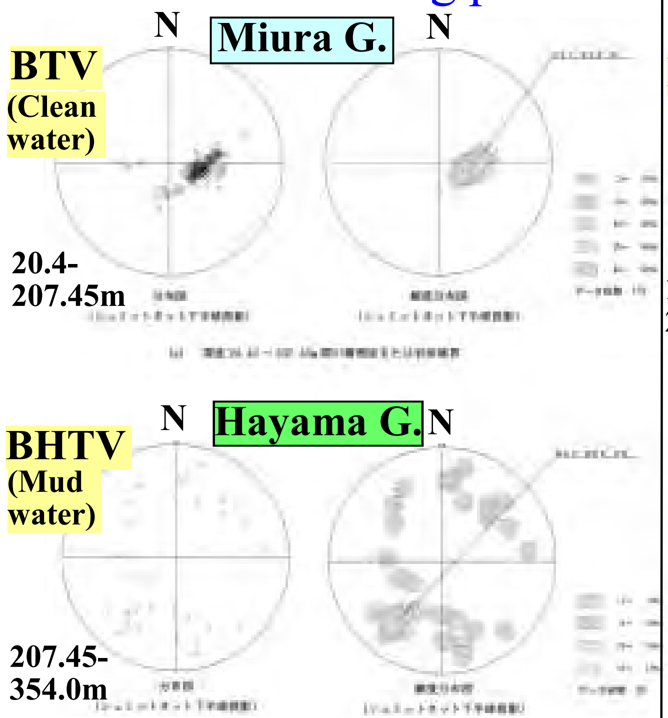

Schmidt's net projection of bedding planes (lower hemisphere)

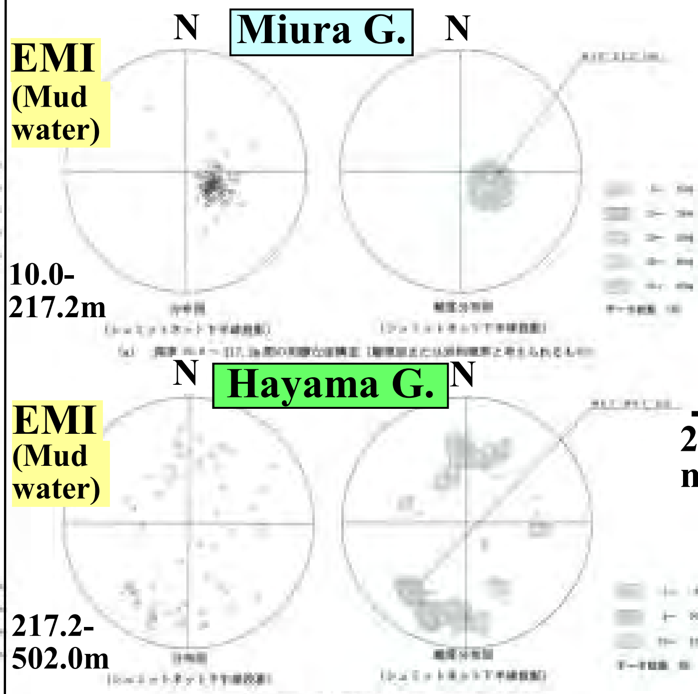

Schmidt's net projection of bedding planes (lower hemisphere)

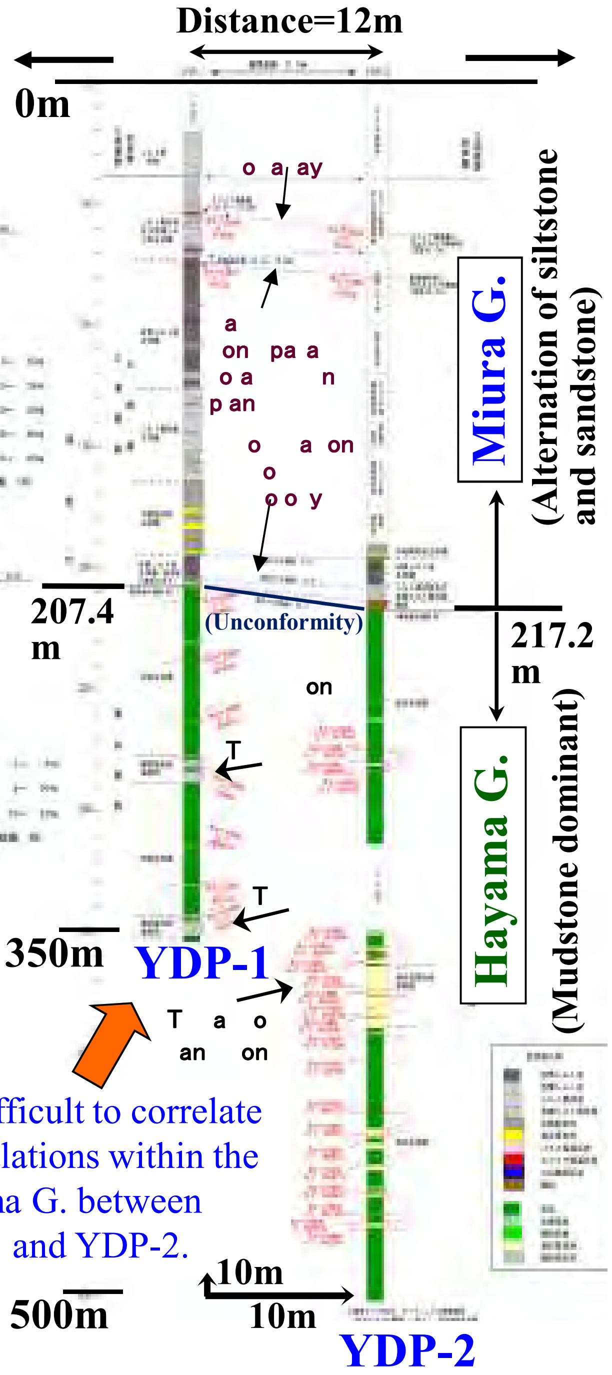

It is difficult to correlate intercalations within the Hayama G. between YDP-1 and YDP-2.

Based on the correlation of bedding planes through the observations of borehole wall and core, it is concluded that..

- **Miura G.:** Bedding planes are gently dipping westward, and it is easy to correlate lithology between two boreholes.
- **Hayama G.:** Bedding planes are moderately to steeply dipping (unevenness in dipping direction), and it is difficult to correlate intercalations within mudstones between two boreholes.

Information for establishing stratigraphy from microfossil biochronology

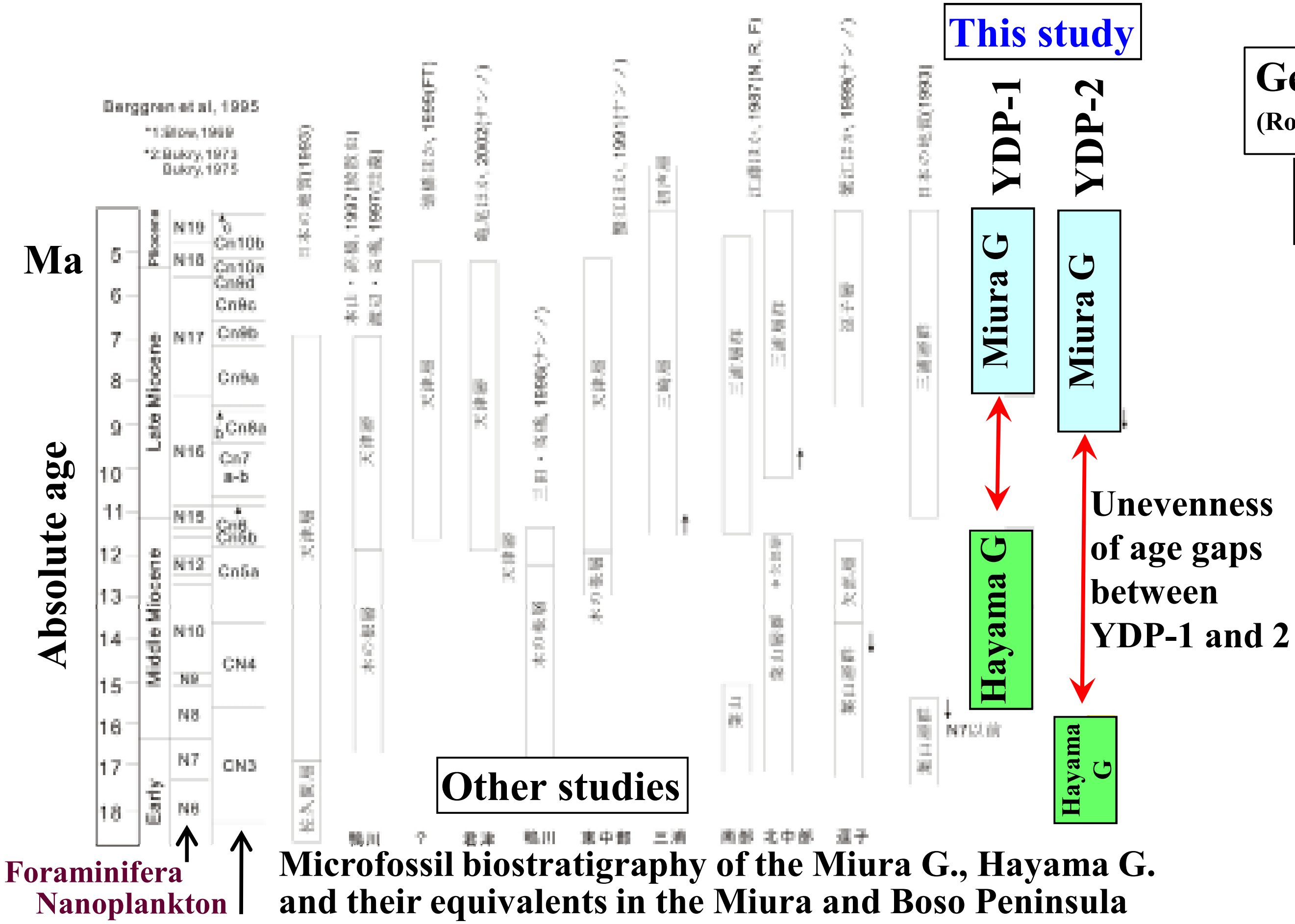

Microfossil biostratigraphy of the Miura G., Hayama G. and their equivalents in the Miura and Boso Peninsula

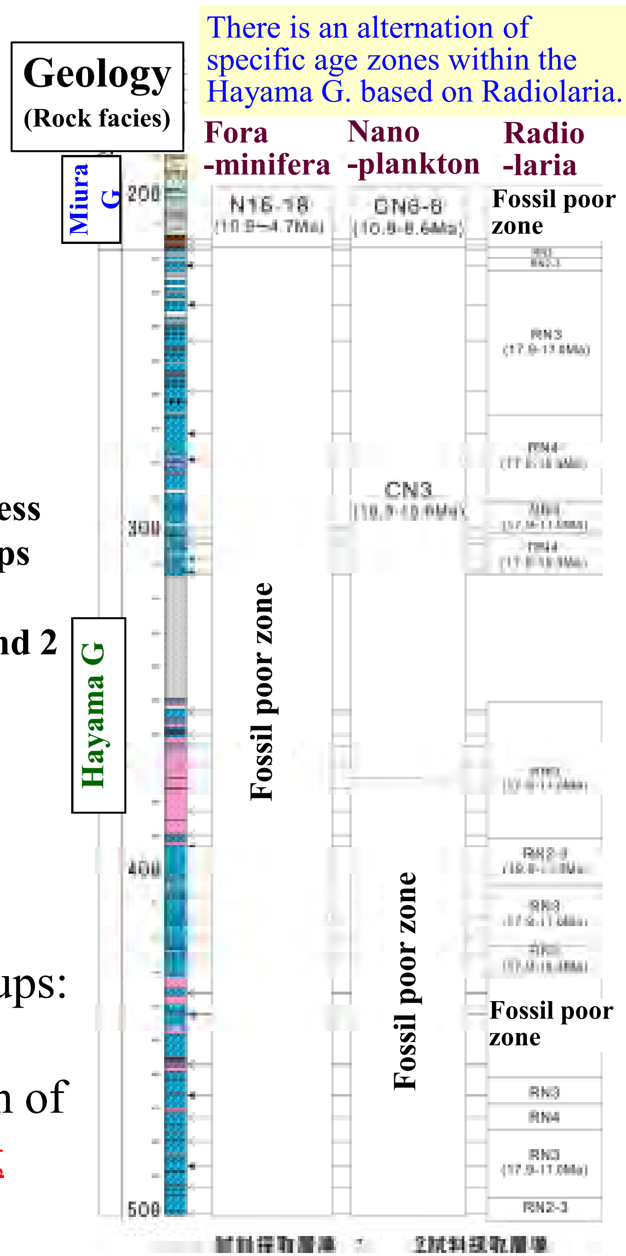

Microfossil biostratigraphy of the Hayama G. in YDP-2

- There is an unconformity between the Miura and Hayama groups: <u>unevenness of age gaps between YDP-1 and YDP-2.</u>
- Radiolarian biostratigraphy revealed that there is an alternation of specific age zones within the the whole Hayama G.: <u>indicating complicated geological structure, even though we can not recognize any fault crushed zone between each of units.</u>

Geological structure model after the results of borehole surveys

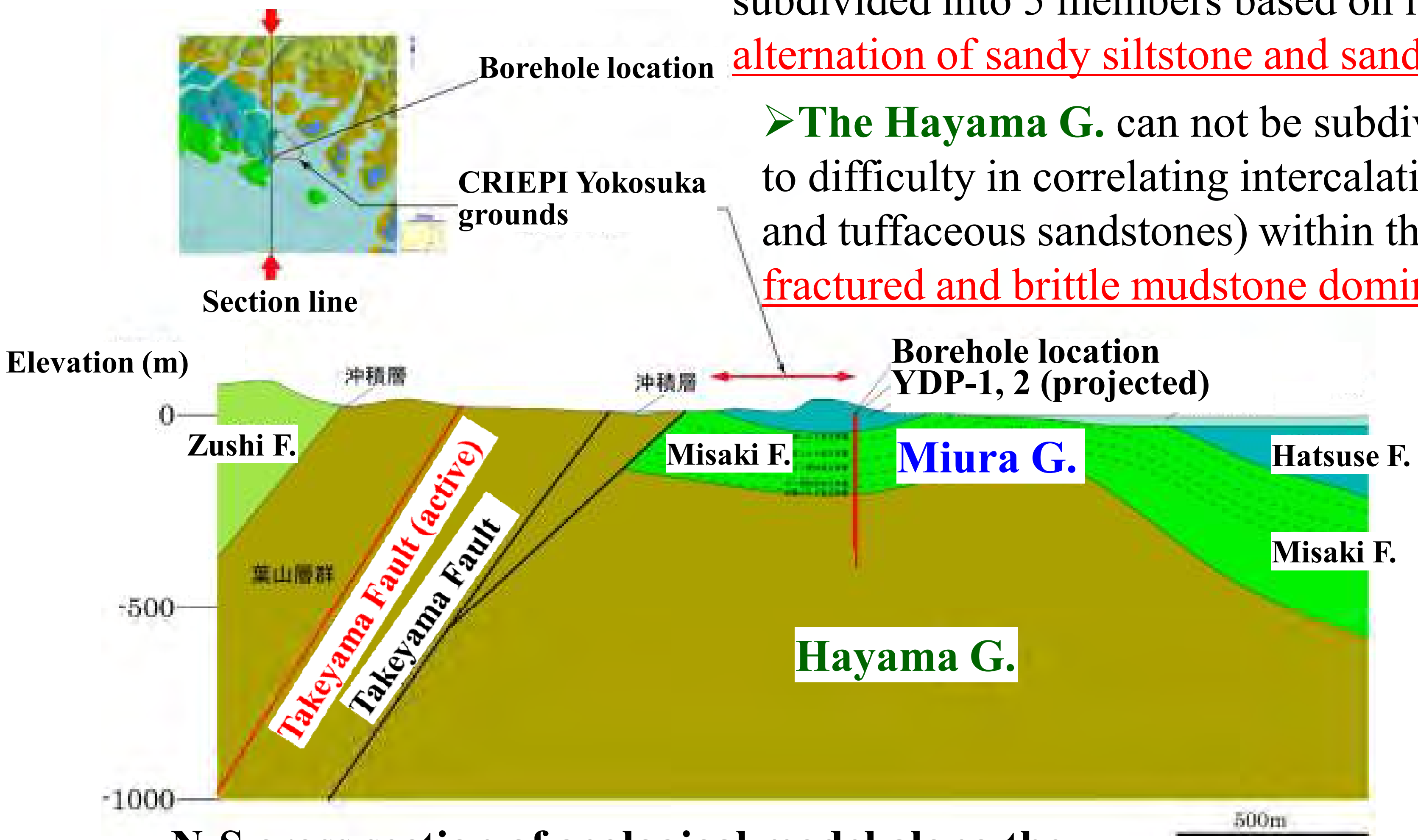

- **The Miura G.** is divided into the Hatsuse and Misaki Formations, and the Misaki F. is subdivided into 5 members based on lithology: alternation of sandy siltstone and sandstone.
- **The Hayama G.** can not be subdivided due to difficulty in correlating intercalations (tuffs and tuffaceous sandstones) within the group: fractured and brittle mudstone dominant.

N-S cross section of geological model along the western margin of the CRIEPI Yokosuka grounds

Geochemical characteristics of rocks of the Miura and Hayama groups

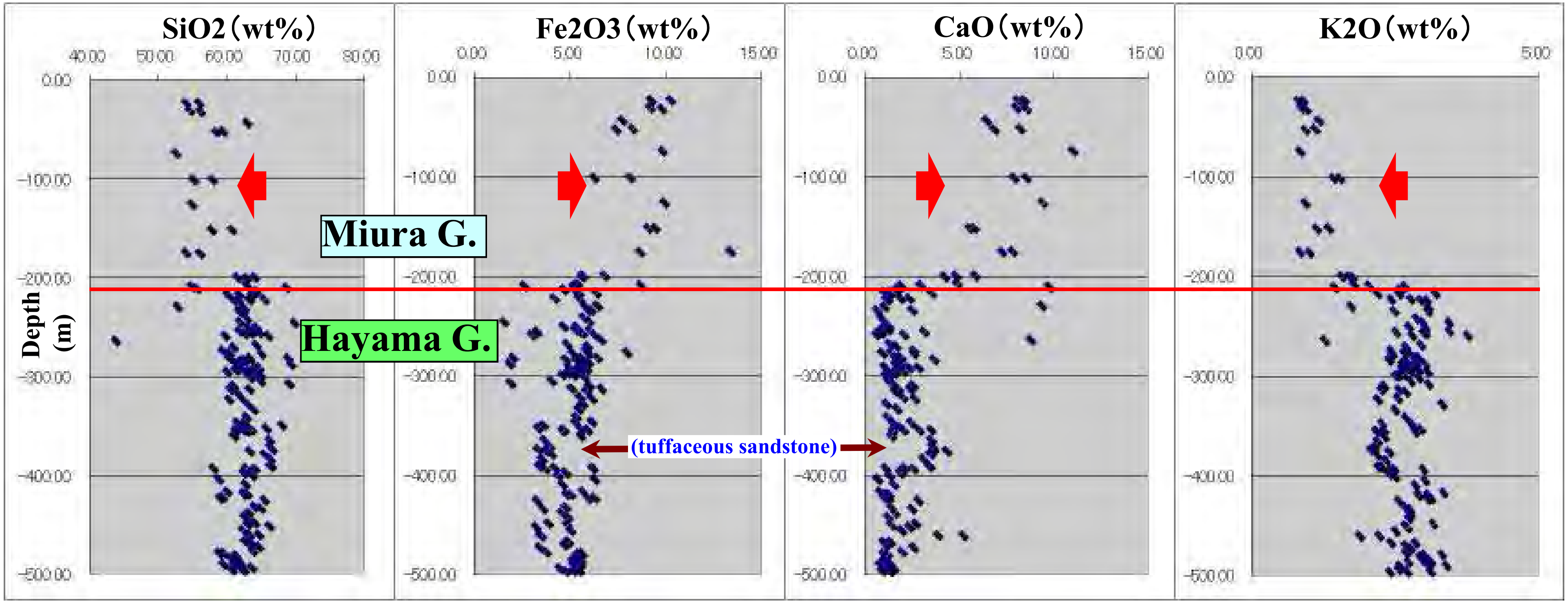

Comparison of bulk rock chemistry (extracted) of the Miura and Hayama groups

Generally, the chemistry of both groups has igneous (volcanic clastic) characteristics.

- **The Miura** shows intermediate (andesitic), **the Hayama** shows intermediate to acidic.
- **The Miura** is characterized by low SiO_2, K_2O and high Fe_2O_3 (total), CaO content, as compared with the Hayama.
- **The Miura's** characteristics rich in CaO coincide with the occurrence of fossils and calcites (possibly have also influenced water chemistry in the Miura).
- There is not remarkable difference in chemistry of mud and intercalations within the Hayama.

Characterization of rock quality of the Miura and Hayama groups

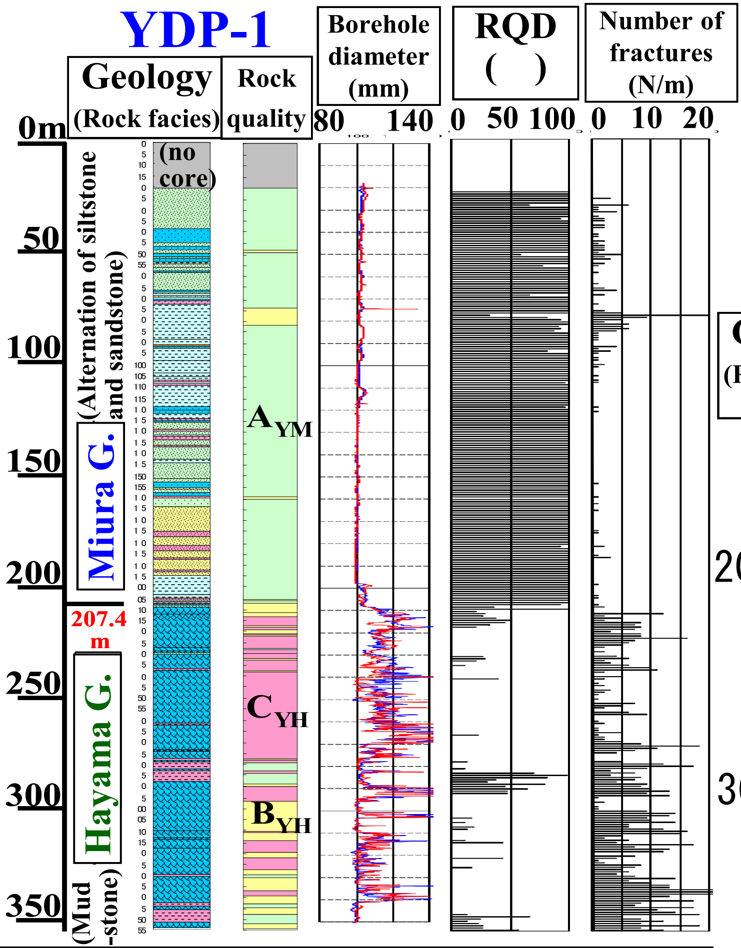

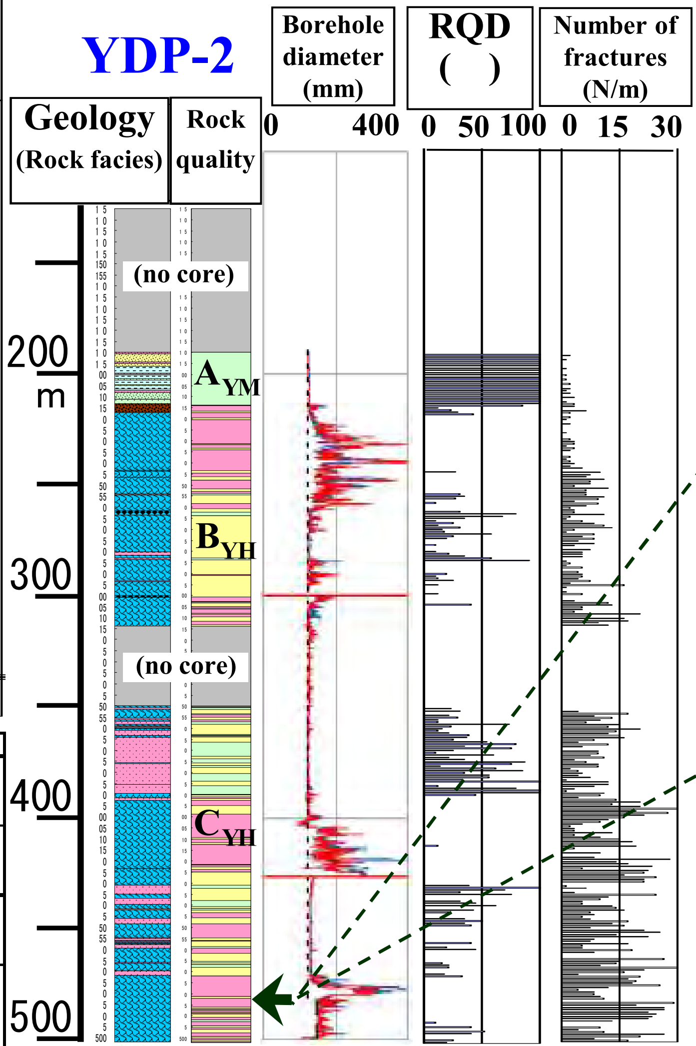

(Number of fractures: countable or detectable fractures except closed and artificially generated ones)

In the Hayama G., there is clear correlation between Class C rock (rudaceous or clayey) and the sections of large borehole diameter after drilling (borehole breakout).

➤Miura G.:

- Class: A (Columnar)
- Fracture: very few

➤Hayama G.:

- Class: B (Fragmentary) or C (rudaceous to clayey)
- Fracture: a large number of microfractures

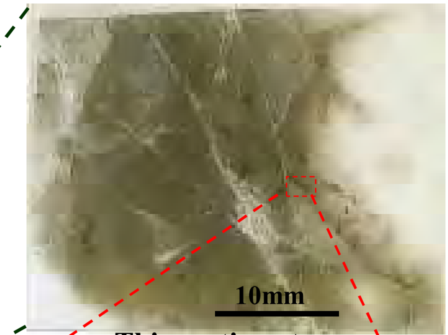

Thin section at around G.L.-482m

a	a o o k a y
a	o n y amm n a y y amm n a a y a kn an a y na n a n a a mo an a n m
a	a n o o k am a a an a o a y a o a n n m n a ok n y n p n y no p n n on a n y
ayama	o n y amm n an a y a a y kn o ma n o mna ap
ayama	a n o o k am a a an a m n a y o o ma n o mna ap a y ok n y amm n a o o k
ayama	a o o ay y o (n n o o)

Physical properties of the Miura and Hayama groups

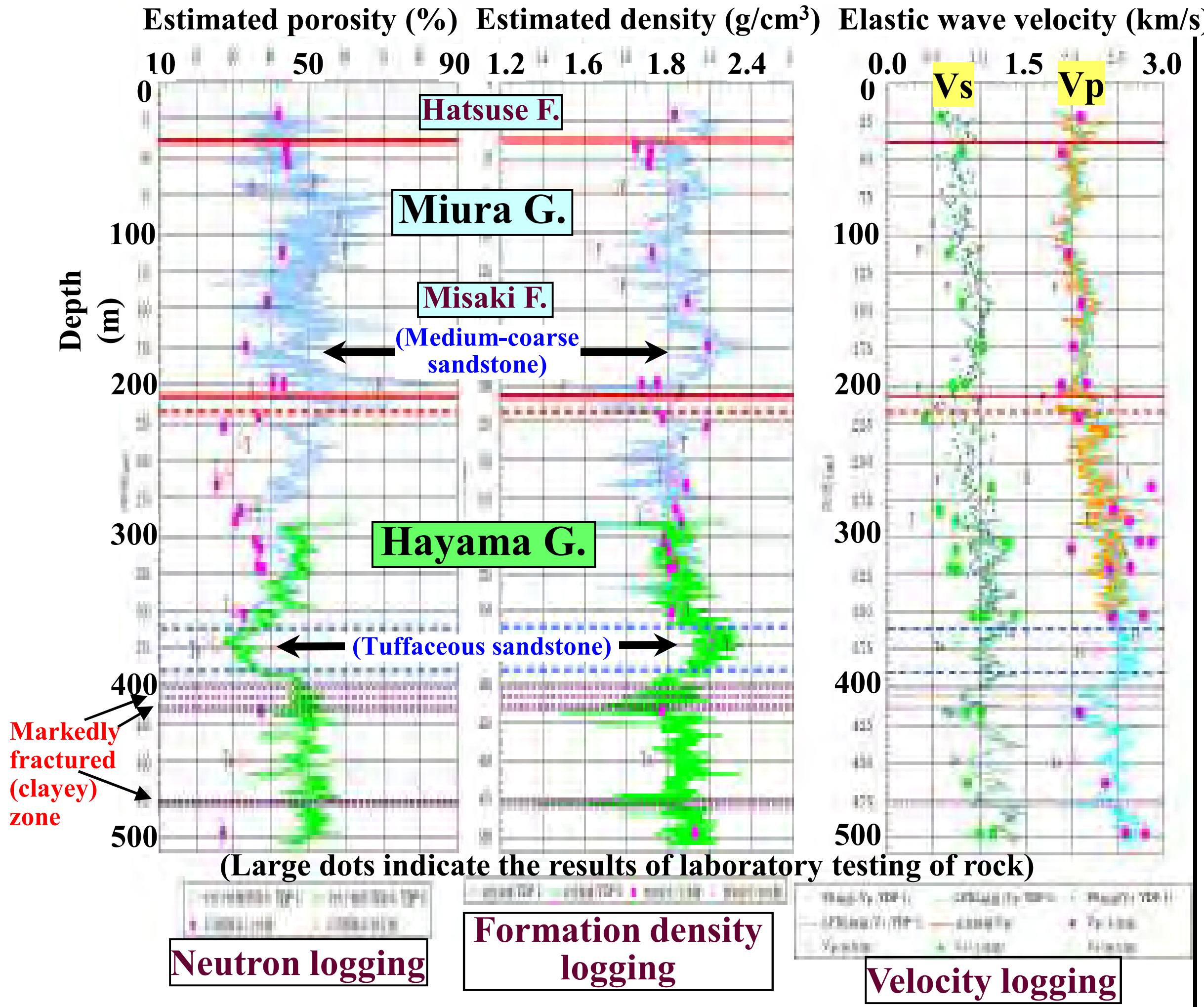

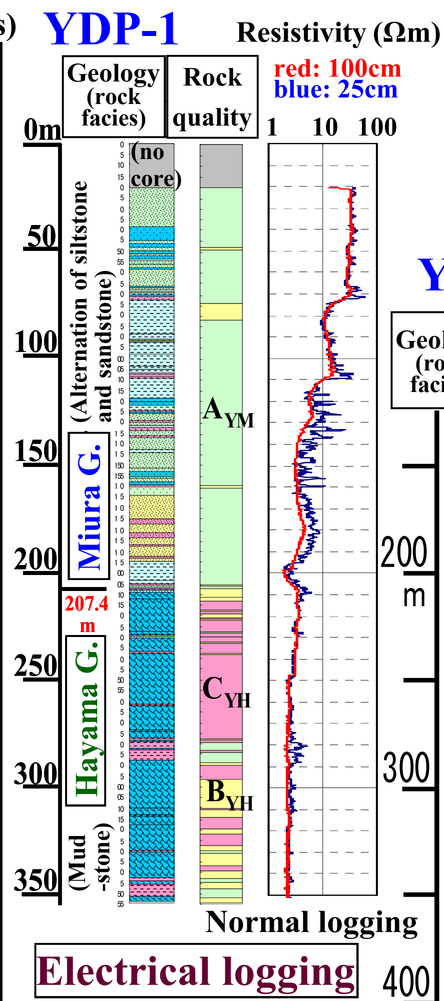

Generally, resistivity drops into a few Ωm stepwise from the surface with depth.
⇒possibility of a reflection of lithology and water chemistry.

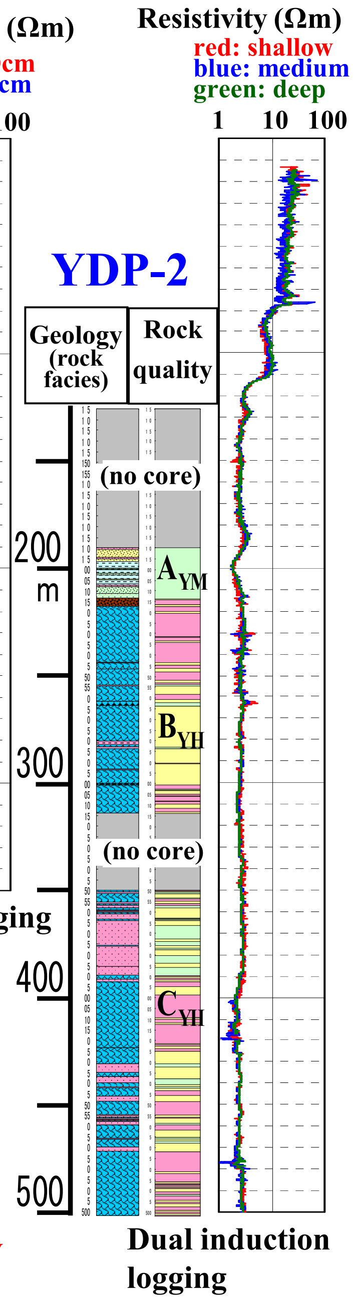

- ➢Physical properties of **the Miura G.** are characterized by higher porosity and lower P-wave and S-wave velocity (as compared with the Hayama G.).
- ➢Intercalations of sandstone within both the Miura and Hayama show lower porosity and higher density (as compared with siltstone or mudstone).
- ➢Markedly fractured (clayey) zones within the Hayama are characterized by smaller density and smaller P-wave and S-wave velocity.

Interpretation of high velocity of the Hayama as compared to the Miura

(In terms of understanding rock mechanical properties)

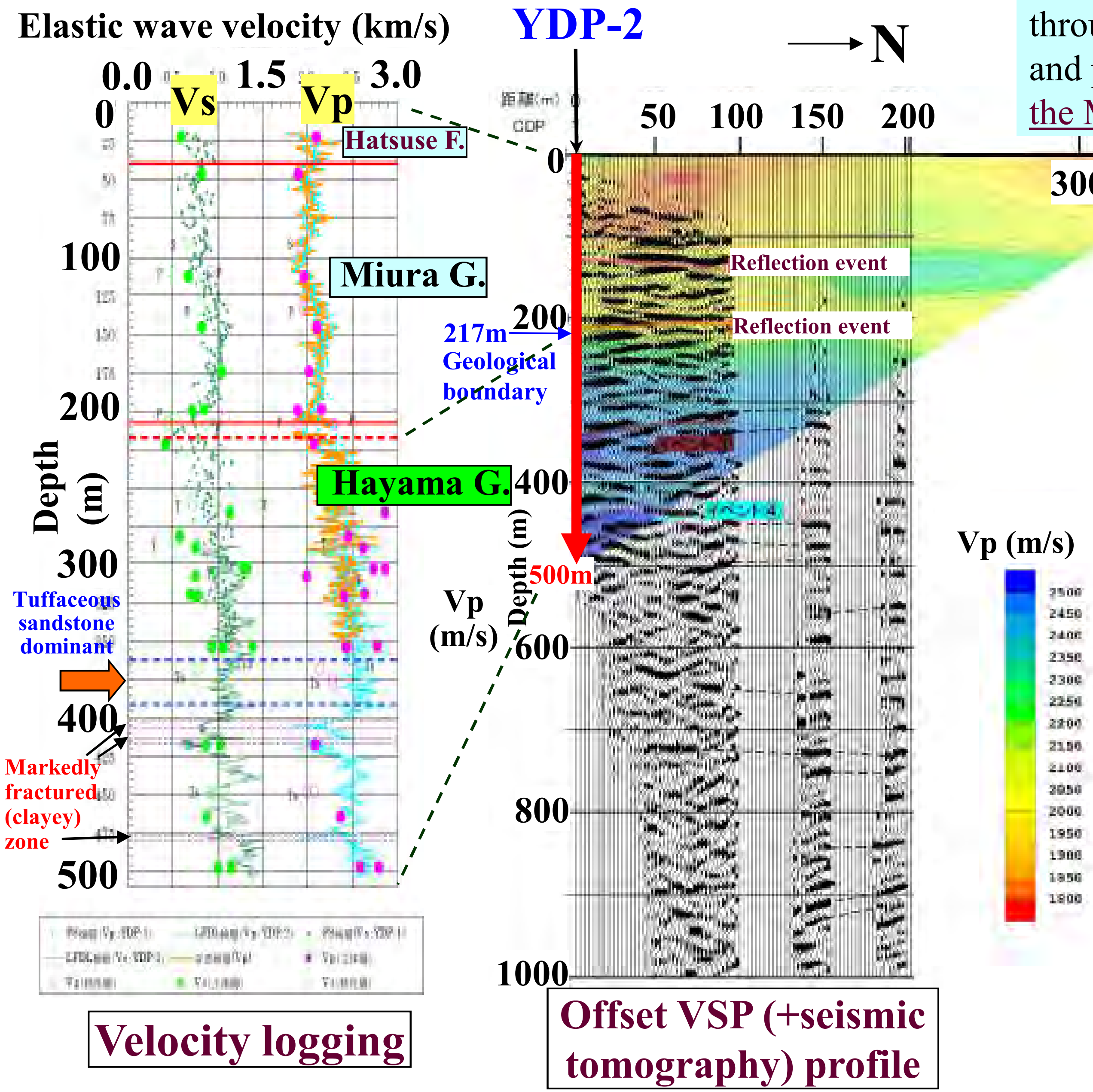

P and S wave velocity obtained through both geophysical logging and prospecting indicates: the Miura G. < the Hayama G.

- Under overburden pressure, rocks are tightly engaged through fractures in the Hayama G. even though there are a large number of fractures as a whole and also immanent microfractures in a rock specimen.

- On the other hand, the overburden pressure is once released, e.g. through drilling, fractures are opened and the core of the Hayama G. becomes fragmentary or rudaceous in shape (brittle).

Issues of in situ borehole tests related to rock mechanical properties

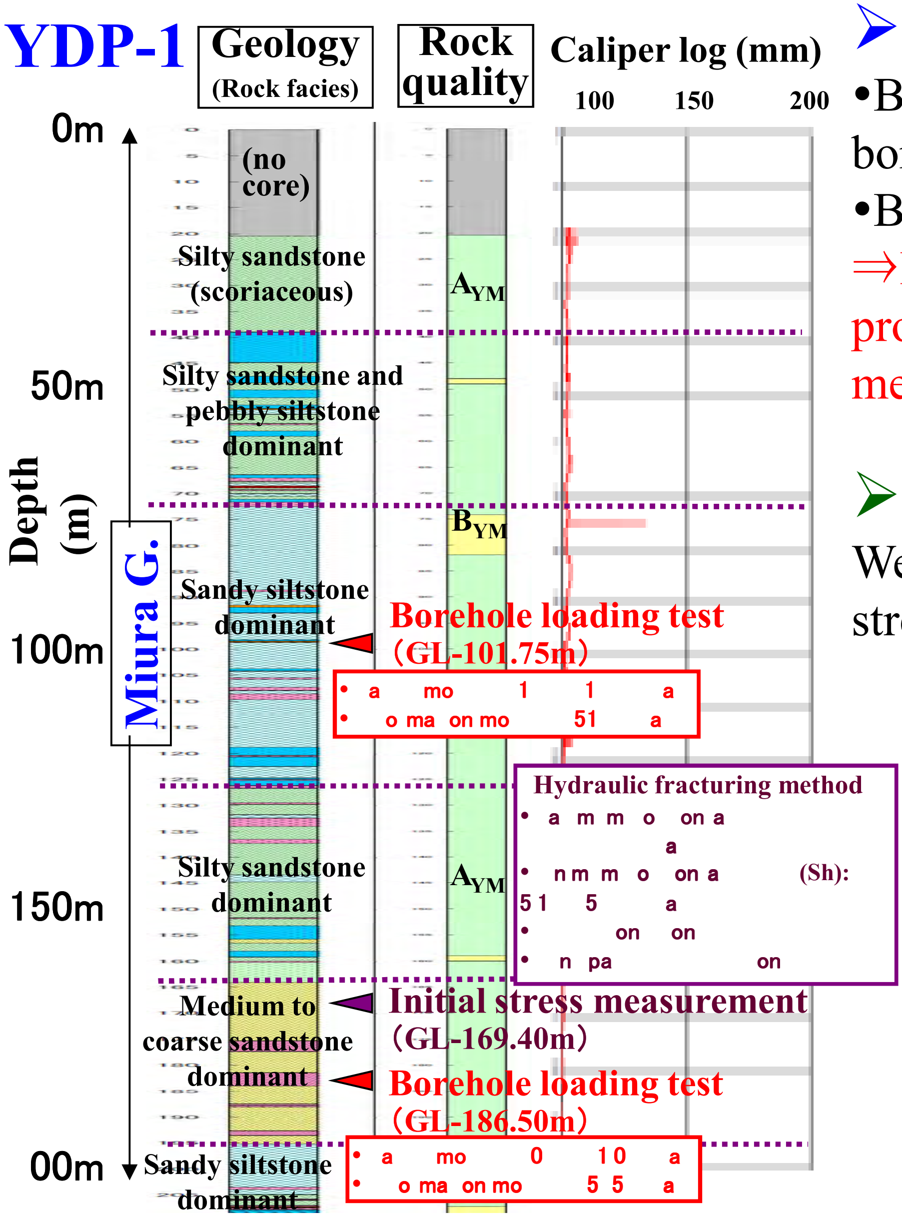

Result of in situ borehole tests related to rock mechanical properties at YDP-1

➢Miura G. (at YDP-1):

•Borehole wall: stable (possible to clean the borehole wall with fresh water)

•Borehole breakout: rare (caliper log data)

⇒In situ borehole tests related to rock mechanical properties (borehole loading test and initial stress measurement) were conducted shallower than 200m.

➢Hayama G. (at YDP-1 and 2):

We skipped in situ testing of rock mechanical and stress for the Hayama G. The reason is the following.

The possibility of tests

➢Borehole breakout: frequent sections of large borehole diameter after drilling (> ca. 140 mm = the maximum permissible diameter of test tools)

➢Risk of test tools being stuck caused by borehole wall collapse: high (because of unstable borehole wall reflecting immanent microfractures and in some parts the presence of swelling clay within the Hayama G.)

The quality of obtained data

➢Possibility of removing mud cake: unrealistic (from the viewpoint of maintaining borehole wall)

Rock mechanical properties of the Miura and Hayama groups

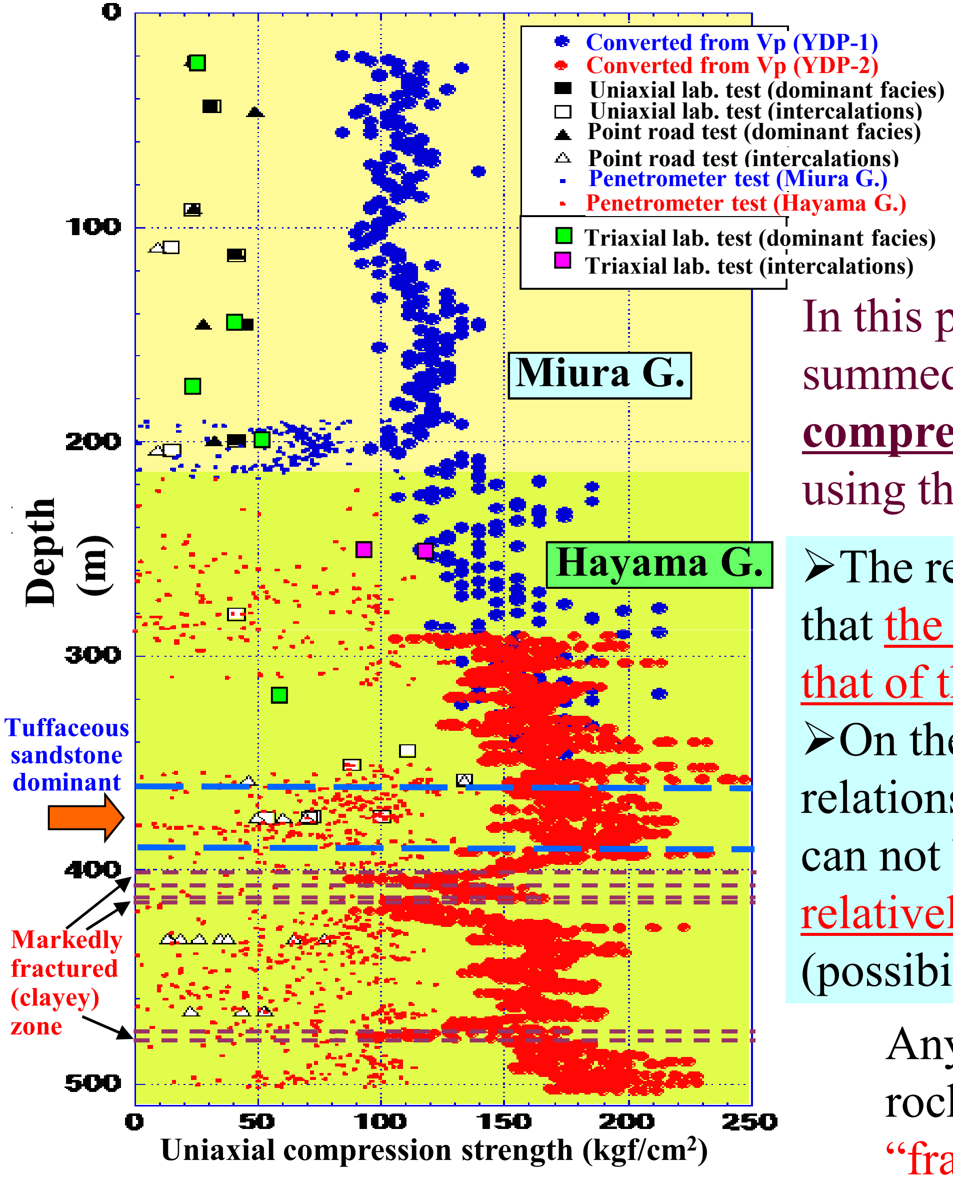

Comparison of rock mechanical properties ("converted values as uniaxial compression strength" from various tests)

- **In situ borehole logging: Velocity logging (Vp)**
- **Lab. tests: Uniaxial and triaxial compression tests, point road test, pnetrometer test**

In situ testing of rock mechanical and stress for the Hayama G. was skipped because of difficulty in ensuring the quality of testing.

In this phase, rock mechanical properties were roughly summed up based on **"converted values as uniaxial compression strength"** (through empirical formulas) using the results of various lab. tests and also loggings.

- The results of velocity logging suggest a possibility that the rock strength of the Hayama G. is higher than that of the Miura G. under the confining pressure.
- On the other hand, such clearly higher or lower relationship between the Miura and Hayama Groups can not be recognized for the results of lab. tests: relatively low for test specimens of the Hayama G. (possibility of the effects of immanent microfractures.)

Anyway we have not obtained directly the real rock strength property data of the main body of "fractured mudstone" (Hayama G.) which is fragmentary or rudaceous in core shape.

Issues of lab. tests of rock mechanical properties of the Hayama G.

- Specimens for rock mechanical strength tests of the Hayama G. can only be obtained from columnar core usually corresponding to intercalations (tuffs and tuffaceous sandstones), not the main rock facies (mudstones).
- As for a uniaxial compression test (under no confining pressure), the test is not concluded successfully in some cases because of the effects of microfractures within the rock specimen. ⇒It seemed that a triaxial compression test were effective.

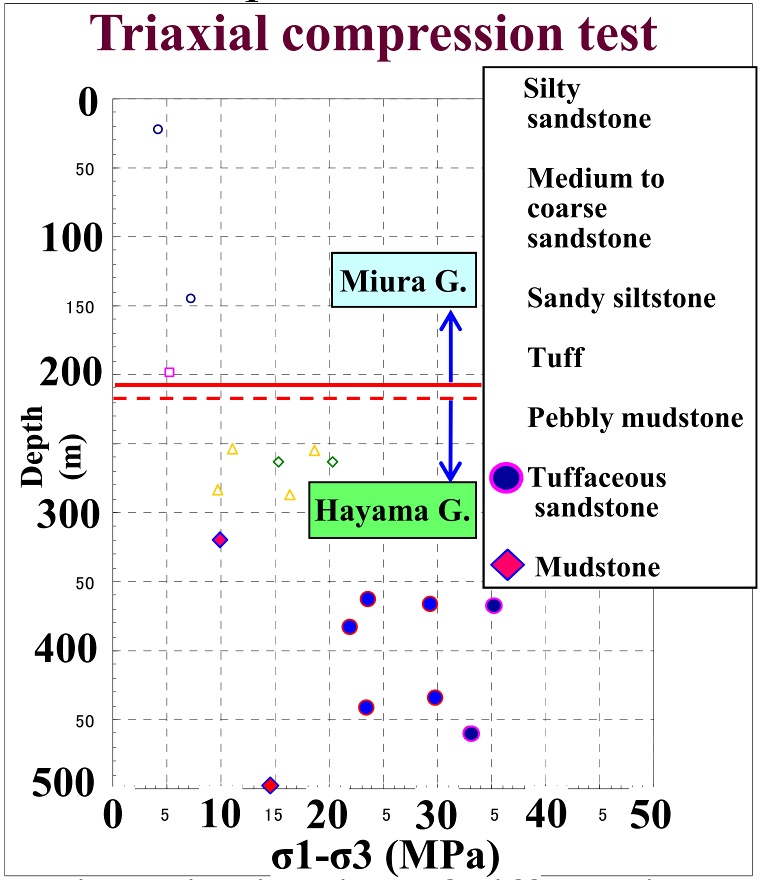

Vertical distribution of differential stress
(compression strength under confining pressure)

- As for a triaxial compression test, it is inevitable to adopt a multiple-step loading test to obtain c' and φ' for a single rock specimen, because of the difficulty in obtaining two or more specimens from the same rock facies at the same depth.
- However in reality, multiple-step loading does not work effectively under higher confining pressure for rock specimens obtained at deeper part, because of the limit of pressure resistant capacity of the test apparatus.

⇒Nevertheless, the results of single-step loading tests indicate clearly high rock strength property of the Hayama G. under overburden pressure. (→at least for intercalations.)

Hydraulic properties of the Miura and Hayama groups

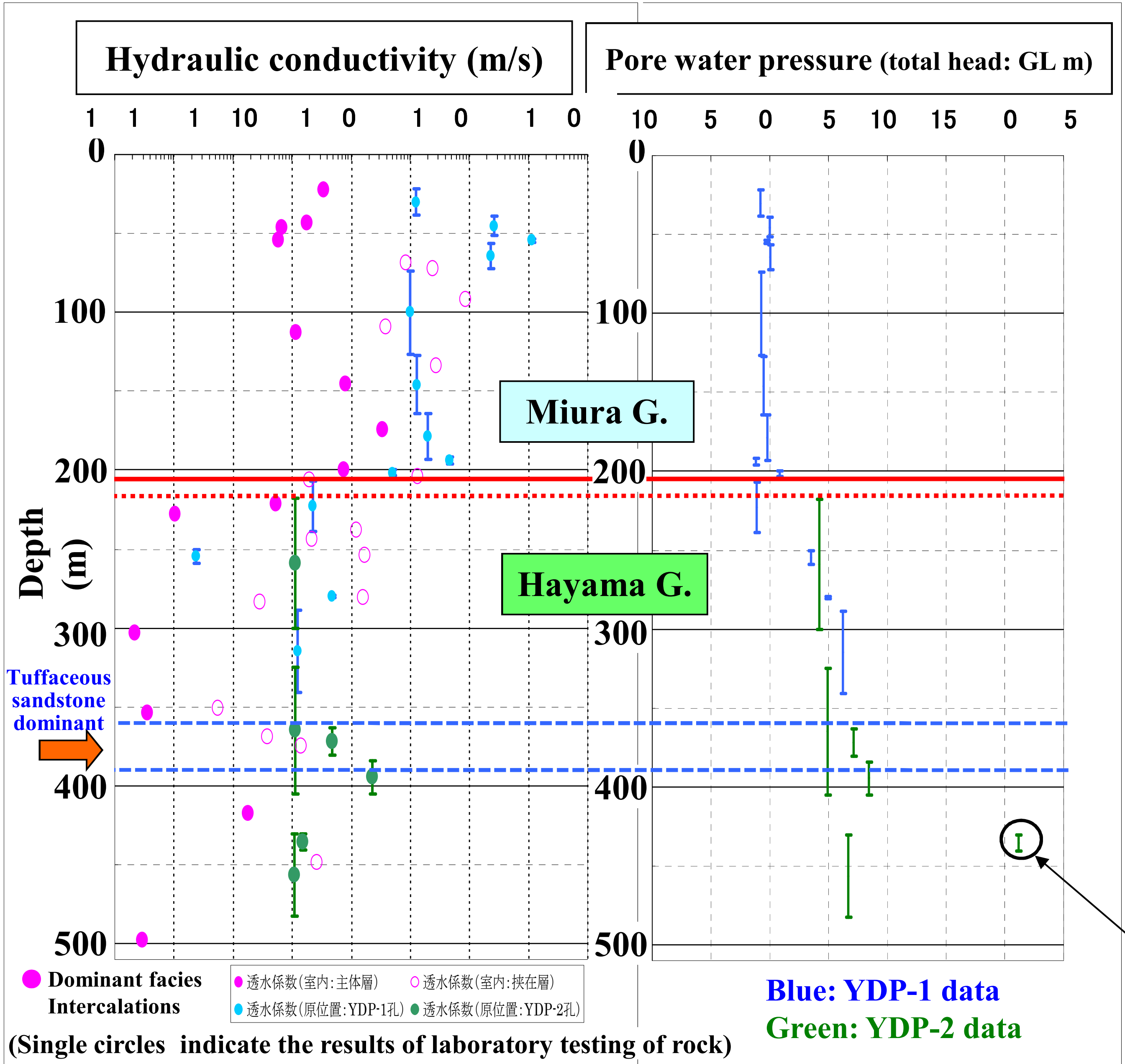

Hydraulic conductivity and pore water pressure based on hydro-test

Hydraulic conductivity

- **Miura G.:**
  order of 10^{-7} m/s
- **Hayama G.:**
  order of 10^{-9} m/s

(Hydrauric conductivity obtained through lab. tests has scattering distribution around values of in situ tests or deviates toward the lower conductivity side)

Pore water pressure (total head)

- **Miura G.:**
  hydrostatic pressure
- **Hayama G.:**
  higher than the hydrostatic pressure (Miura).

(Estimated pore water pressure had been decreasing gradually during a sequential test in this section.)

Geochemical properties of groundwater (EC and major ion distribution)

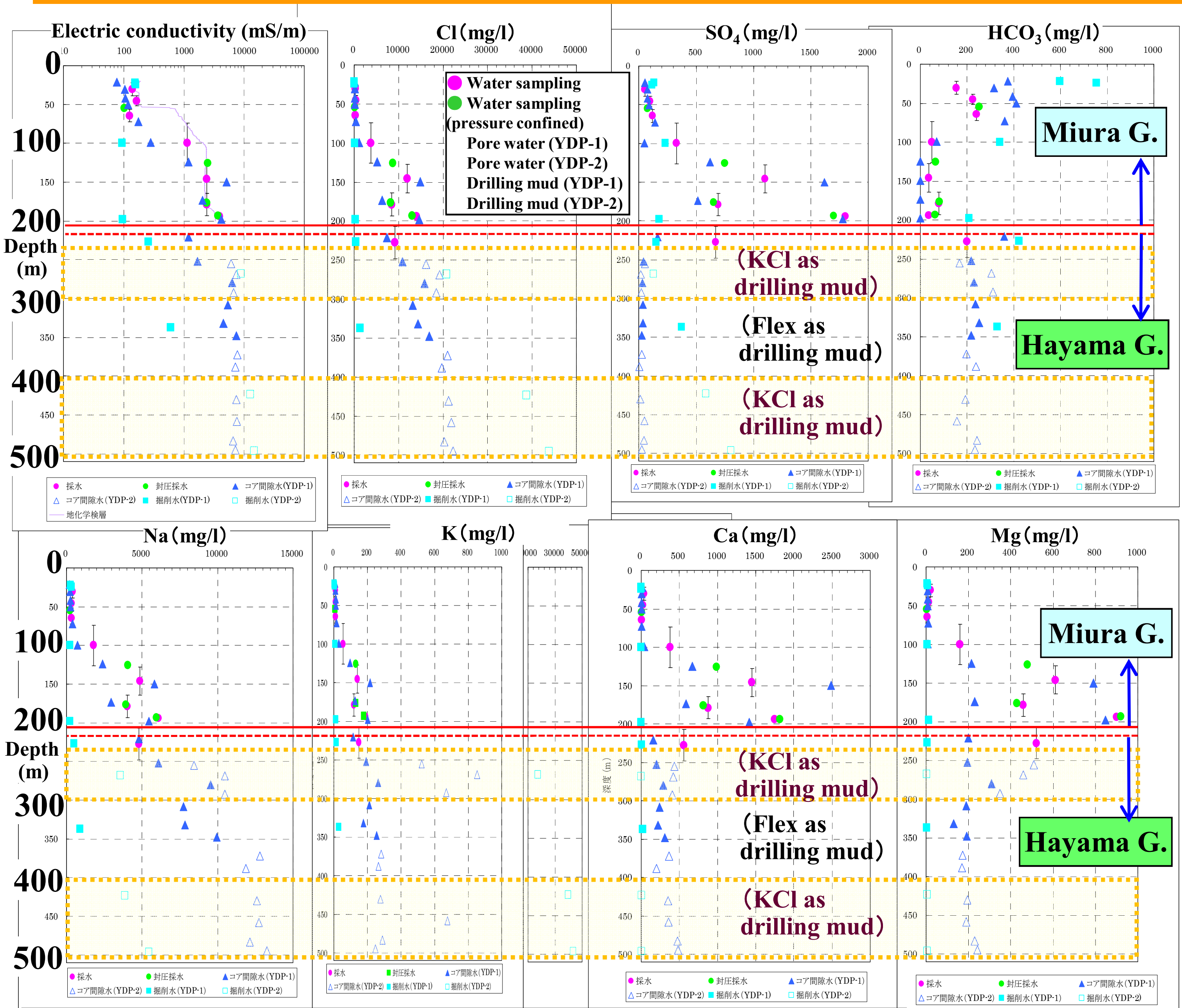

Water was sampled through in situ sampling or pore water squeezing.

- Groundwater samples showing sufficiently few effects of drilling mud had not been obtained for a realistic period through water sampling for the low permeable Hayama G.
- In such case, a pore water squeezing method of core samples was available for obtaining water samples.
- Chemical data showing relatively fewer effects of drilling mud suggest the following tendency.

➢ **The upper part:**
(shallower than ca. 100m)
⇒Fresh water

➢ **The lower part:**
(deeper than ca. 100m)

- Salinity increases to sea water level with depth.
- There is a part showing high concentrations of Ca, Mg, and SO_4 within the Miura G. as compared with other parts.

Summary: establishment of site descriptive models

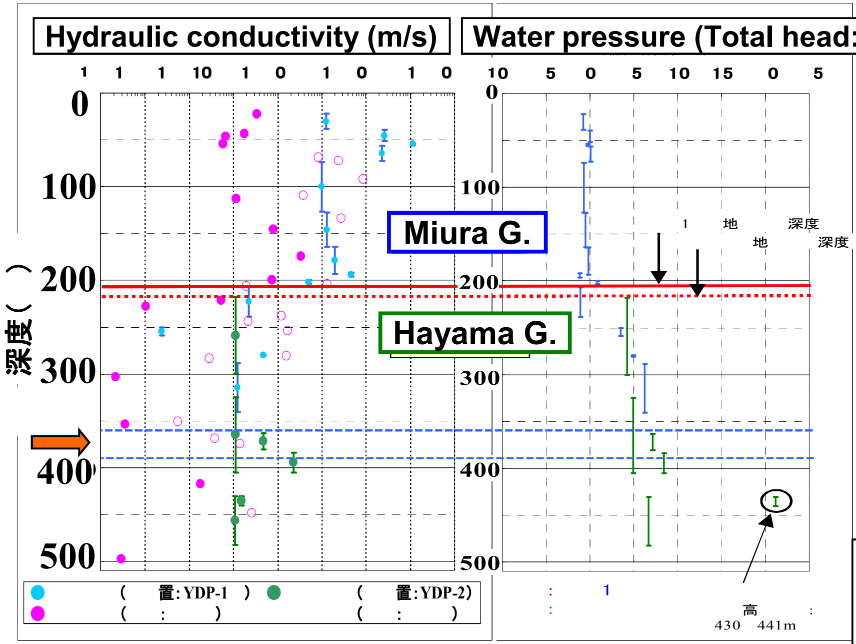

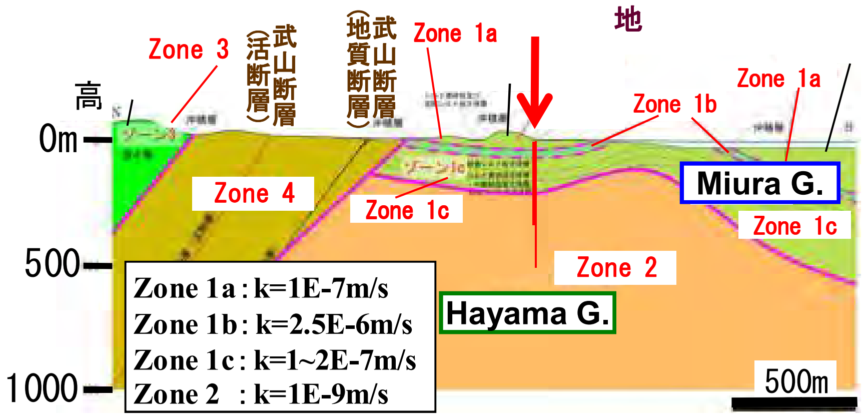

Hydrogeological structure model

Division of groundwater flow system (around boreholes):

- ➢GL-0 100m (shallower Miura): Rainwater (higher circulation)
- ➢GL-100 200m (deeper Miura): Rainwater + Seawater (high mobility)
- ➢GL-200 300m (shallower Hayama): Rainwater + Seawater + Fossil seawater
- ➢Deeper than GL-300m (main Hayama): Fossil seawater (higher stagnancy)

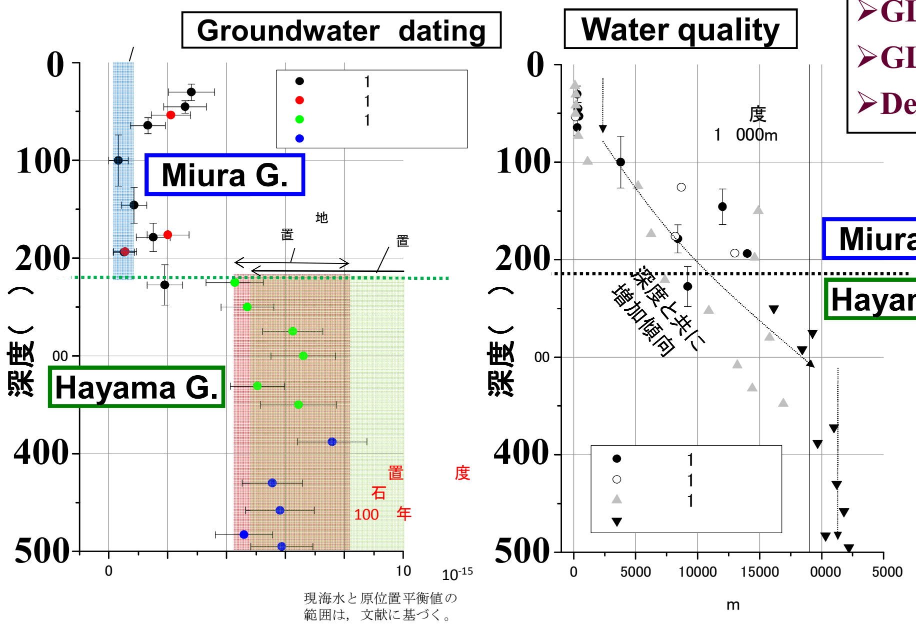

^{36}Cl/Cl distribution with depth

Cl concentration with depth

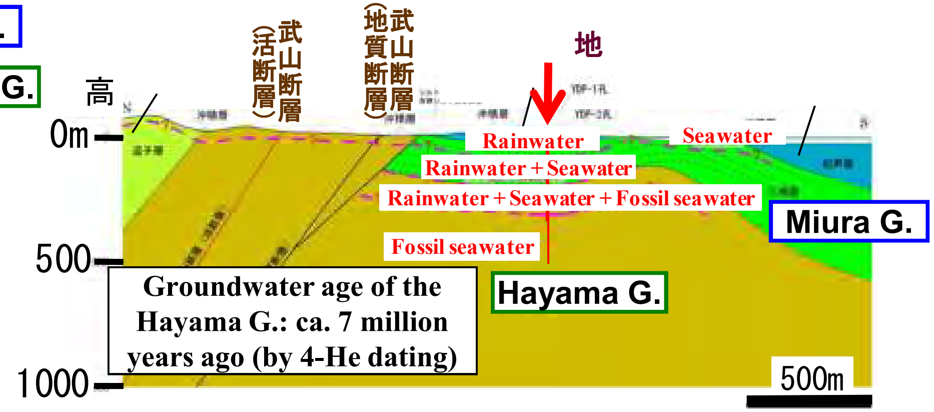

Geochemical properties of groundwater model